

## Molecular-dynamics study of a three-dimensional one-component model for distortive phase transitions

T. Schneider and E. Stoll

*IBM Zurich Research Laboratory, 8803 Rüschlikon, Switzerland*

(Received 15 August 1977)

Molecular-dynamics results simulating a canonical ensemble with nearly conserved energy are presented and discussed for a one-component model exhibiting a distortive continuous-phase transition. Our results demonstrate (i) that the static properties are consistent with the universality hypothesis; (ii) the formation of clusters; (iii) second sound in a temperature window below  $T_c$ ; (iv) central peaks due to the cluster dynamics and heat diffusion; (v) that the critical slowing-down data are consistent with the universality hypothesis for dynamic critical phenomena; and (vi) envelope solitonlike heat-pulse propagation in the second-sound regime.

### I. INTRODUCTION

This paper is concerned with a three-dimensional one-component model for distortive-phase transitions. It may also be viewed as a set of harmonically coupled oscillators with quartic anharmonic and identical single-particle potentials. It belongs to the family of models which have been used with remarkable success to elucidate the critical properties associated with ferro- and antiferrodistortive phase transitions.<sup>1</sup> As far as the static critical properties are concerned, it is equivalent to a one-component continuous spin model<sup>2</sup> which reduces in a certain limit to the Ising model.<sup>3</sup> According to the universality hypothesis for static properties, one therefore expects that the system belongs to the Ising universality class. Similarly, invoking the universality hypothesis for dynamic critical phenomena,<sup>4</sup> the dynamic critical behavior should be essentially that of the time-dependent Ginzburg-Landau (TDGL) model with conserved energy. The requirement of energy conservation reflects the fact that our model is defined by a Hamiltonian.

It is not the main purpose of the present paper to study the critical phenomena occurring close to the phase transition. Our main concern is the excitation spectrum, the nature of its dependence on temperature variation, and the presence of an order parameter. Nevertheless, some critical properties will be studied. Our main motivation for the present study was to extend our previous work on the two-dimensional version of the model<sup>5,6</sup> to a three-dimensional system and, in addition, to modify the molecular-dynamics technique. The modified molecular-dynamics technique employed here allows us to simulate a canonical ensemble with nearly conserved energy. On this basis, it would be possible to study the effects of the coupling between energy and displacement fluctuations, heat diffusion, second sound, and

heat-pulse propagation. The following main results are obtained:

(i) The static critical properties are consistent with the universality hypothesis. (ii) The formation of clusters of locally ordered regions is demonstrated. (iii) Optical-mode second sound is found in a temperature window below  $T_c$ . At the upper limit it becomes overdamped and goes over to thermal diffusion. (iv) In the vicinity of  $T_c$ , a central peak (CP) is found. For wave vectors  $\vec{q} = \vec{0}$  it is a superposition of a CP due to the cluster dynamics and a CP due to heat diffusion. (v) Above and close to  $T_c$ , the central peak in the displacement spectral density originates entirely from the cluster dynamics, because the coupling between order parameter and energy fluctuations vanishes. (vi) The critical slowing-down data are consistent with the universality hypothesis for dynamic critical phenomena. (vii) Envelope solitonlike heat-pulse propagation under second-sound conditions is demonstrated.

In Sec. II, we define the model, the dynamic variables, and the conservation laws. Moreover, to approach the problem of excitations, we sketch Mori's treatment<sup>7,8</sup> of the correlation functions, which permits a discussion of the excitations associated with small-amplitude oscillations. Finally, we consider the implications of large-amplitude oscillations, which may give rise to solitary waves, and study the possibility of solitonlike heat-pulse propagation.

The modified molecular-dynamics technique is described in Sec. III. The details of the algorithm used and of the generation of the random force are given in an Appendix. In Sec. IV, we present some of the numerical results. They include (a) static critical properties; (b) dynamic properties such as second sound, heat diffusion, central peaks, phonons, large-amplitude oscillations, and critical slowing down; and (c) envelope solitonlike heat-pulse propagation in the second-sound regime.<sup>9,10</sup>

## II. MODEL AND THEORETICAL DESCRIPTION

In this section, we define the model, the dynamic variables of interest, and the conservation laws. In addition, we shall outline Mori's treatment of correlation functions,<sup>7,8</sup> where one takes into account, right from the beginning, all relevant variables which might introduce poles, including the hydrodynamic ones. This discussion will include the second-sound phenomenon.<sup>11,12</sup> Finally, we study the possibility of solitonlike heat-pulse propagation.

### A. Model, dynamic variables, and conservation laws

The Hamiltonian of the ferrodistorptive model is

$$\mathcal{H} = \sum_l \frac{P_l^2}{2M} + \frac{A}{2} \sum_l X_l^2 + \frac{B}{4} \sum_l X_l^4 - C \sum_{\langle l, l' \rangle} X_l X_{l'}, \quad (1)$$

$l$  labels the particle with mass  $M$  in the  $l$ th unit cell.  $P_l$  and  $X_l$  are momentum and displacement with respect to a rigid cubic primitive reference lattice.  $M$ ,  $A$ ,  $B$ , and  $C$  are model parameters, which are chosen as

$$A = -1, \quad B = \frac{1}{3}, \quad C = \frac{1}{6}, \quad M = 1. \quad (2)$$

Here, we have adopted the same units as in Ref. 6. This choice of the model parameters guarantees that at  $T = 0$  the order parameter given by

$$X_l^2 = (12C - A)/B \neq 0 \quad (3)$$

does not vanish. Consequently, the system will undergo a ferrodistorptive phase transition at some  $T = T_c > 0$ .<sup>13</sup>

To describe the static and dynamic properties of the system, we shall consider the following variables:

$$P(\vec{q}) = \frac{1}{N^{1/2}} \sum_l P_l e^{i\vec{q} \cdot \vec{R}_l}, \quad (4)$$

$$X(\vec{q}) = \frac{1}{N^{1/2}} \sum_l (X_l - \langle X_l \rangle) e^{i\vec{q} \cdot \vec{R}_l}, \quad (5)$$

$$\rho(\vec{q}) = \frac{1}{N^{1/2}} \sum_l \{ \exp - i\vec{q} \cdot [\vec{R}_l + (X_l, 0, 0)] - \langle \exp - i\vec{q} \cdot [\vec{R}_l + (X_l, 0, 0)] \rangle \}, \quad (6)$$

$$\mathcal{H}(\vec{q}) = \frac{1}{N^{1/2}} \sum_l (\mathcal{H}_l - \langle \mathcal{H}_l \rangle) e^{i\vec{q} \cdot \vec{R}_l}, \quad (7)$$

where

$$\mathcal{H}_l = \frac{P_l^2}{2M} + \frac{A}{2} X_l^2 + \frac{B}{4} X_l^4 - C \sum_m X_l X_{l+m}. \quad (8)$$

These variables describe momentum, displacement, density, and energy fluctuations, respectively, of wave vector  $\vec{q}$ . The vectors  $\vec{R}_l$

define the direct lattice.

Introducing

$$\delta X_l = X_l - \langle X_l \rangle = X_l - \langle X \rangle, \quad (9)$$

we may rewrite Hamiltonian (1) in the form

$$\begin{aligned} \mathcal{H} = & \sum_l \frac{P_l^2}{2M} + \frac{N}{2} \langle X \rangle^2 \left( A - 6C + \frac{B}{2} \langle X \rangle^2 \right) \\ & + \langle X \rangle (A + B \langle X \rangle^2) \sum_l \delta X_l - C \langle X \rangle \sum_{l,m} (\delta X_l + \delta X_{l+m}) \\ & + \frac{1}{2} (A + 3B \langle X \rangle^2) \sum_l \delta X_l^2 + B \langle X \rangle \sum_l \delta X_l^3 \\ & + \frac{B}{4} \sum_l \delta X_l^4 - C \sum_{l,m} \delta X_l \delta X_{l+m}, \end{aligned} \quad (10)$$

revealing the presence of third-order anharmonicity, below  $T_c$ . The resulting equations of motion are

$$\begin{aligned} -M \delta \ddot{X}_l = & \langle X \rangle (A - 12C + B \langle X \rangle^2) \\ & + (A - 12C + 3B \langle X \rangle^2) \delta X_l + 3B \langle X \rangle \delta X_l^2 \\ & + B \delta X_l^3 + 2C \sum_m (\delta X_l - \delta X_{l+m}). \end{aligned} \quad (11)$$

It then follows that

$$\begin{aligned} -M \langle \delta \ddot{X}_l \rangle = & (A - 12C + B \langle X \rangle^2) \langle X \rangle + 3B \langle X \rangle \langle \delta X_l^2 \rangle \\ & + B \langle \delta X_l^3 \rangle = 0 \end{aligned} \quad (12)$$

or

$$(12C - A)/B \langle X \rangle = \langle X^3 \rangle. \quad (13)$$

Invoking the exact inequality<sup>14</sup>

$$\langle X^3 \rangle \geq \langle X^2 \rangle \langle X \rangle, \quad (14)$$

we find that

$$\langle X^2 \rangle \leq (12C - A)/B - \langle \delta X_l^2 \rangle. \quad (15)$$

We are now prepared to derive certain properties of the dynamic variables. From Eq. (6), we have

$$\begin{aligned} \dot{\rho}(\vec{q}, t) = & i q_x \frac{1}{N^{1/2}} \sum_l X_l e^{i\vec{q} \cdot [\vec{R}_l + (X_l, 0, 0)]} \\ = & i q_x J_{\dot{x}}(\vec{q}, t), \end{aligned} \quad (16)$$

so that  $\dot{\rho}(\vec{0}, t) = 0$ , and the density is therefore conserved because  $\dot{\rho}(\vec{0}, t) = 0$ . The momentum current  $J_{\dot{x}}(\vec{q}, t)$ , however, is not a conserved quantity. In fact, we find

$$\begin{aligned} \dot{J}_{\dot{x}}(\vec{q}, t) = & \frac{1}{N^{1/2}} \sum_l (\ddot{X}_l + i q_x \dot{X}_l^2) \\ & \times e^{i\vec{q} \cdot [\vec{R}_l + (X_l, 0, 0)]} \end{aligned} \quad (17)$$

and, according to Eq. (11),

$$-M \sum_i \ddot{X}_i = \left( N \langle X \rangle + \sum_i \delta X_i \right) (A - 12C + B \langle X \rangle^2) + 3B \langle X \rangle \sum_i \delta X_i^2 + B \sum_i \delta X_i^3, \quad (18)$$

representing the total force. Because the model defined by Hamiltonian (1) is not translationally invariant, the total force does not vanish. Consequently, the momentum current is not conserved because  $\dot{J}_i(\vec{0}, t) \neq 0$ .

From Eqs. (7) and (11), we find for the rate of change of the energy fluctuations

$$\begin{aligned} \dot{\mathcal{H}}(\vec{q}, t) = & 2C \frac{1}{N} \sum_{\vec{q}'} [X(\vec{q} - \vec{q}') \dot{X}(\vec{q}')] \\ & - \dot{X}(\vec{q} - \vec{q}') X(\vec{q}')] F(\vec{q}') \\ & + 2C \langle X \rangle [F(\vec{0}) - F(\vec{q})] \dot{X}(\vec{q}), \end{aligned} \quad (19)$$

where

$$F(\vec{q}) = \cos a q_x + \cos a q_y + \cos a q_z, \quad (20)$$

$a$  being the lattice constant of the cubic primitive reference lattice.  $\dot{\mathcal{H}}(\vec{0}, t)$  is seen to vanish, so that energy is conserved as it should be for a Hamiltonian system. We express this conservation law in the form

$$\dot{\mathcal{H}}(q_x, t) = i q_x J_{\mathcal{H}}(q_x, t). \quad (21)$$

#### B. $n$ -variable theory

To characterize the excitation spectrum, we adopt Mori's treatment of correlation functions.<sup>7,8</sup> It is well known that a perturbative treatment of the anharmonic terms has to treat hydrodynamic singularities correctly.<sup>9,10</sup> These singularities are a consequence of the coupling between the dynamic variable, whose spectral density one wants to calculate, and some further slowly varying dynamic variable. Instead of summing up infinite series of terms in a perturbation expansion, one tries, in the Mori approach, to take into account right from the onset all important slowly decaying dynamic variables which might introduce hydrodynamic poles. Without going into details of such a spectral density matrix formalism, we sketch below the structure of the theory. For details, we refer to Refs. 7 and 8.

We consider the retarded Green's function

$$G_{AA}^+(t) = -i \theta(t) \langle [A^\dagger(t), A] \rangle. \quad (22)$$

Using the identity

$$\begin{aligned} -i \langle [A^\dagger(t), A] \rangle = & + \int_0^{\beta} d\lambda \langle e^{\lambda \mathcal{H}} \dot{A}^\dagger(t) e^{-\lambda \mathcal{H}} A(0) \rangle \\ \equiv & (\dot{A} | A), \end{aligned} \quad (23)$$

Eq. (22) may be rewritten

$$G_{AA}^+(t) = (\dot{A}(t) | A), \quad t > 0. \quad (24)$$

Introducing the Liouville operator

$$A(t) = e^{iL t} A, \quad (25)$$

we find

$$\begin{aligned} G_{AA}^+(z) = & \int_0^{\infty} e^{i z t} (\dot{A}(t) | A) dt \\ = & -(A | A) + (A | \frac{z}{z - L} | A). \end{aligned} \quad (26)$$

With the aid of the projection operator

$$P = |A\rangle \frac{1}{(A|A)} \langle A|, \quad Q = 1 - P, \quad (27)$$

one may rewrite Eq. (26) in the form

$$\begin{aligned} G_{AA}^+(z) = & -(A|A) [z(A|A) + i(\dot{A}|A) + iF_{AA}(z)]^{-1} \\ & \times [i(\dot{A}|A) + iF_{AA}(z)], \end{aligned} \quad (28)$$

where

$$F_{AA}(z) = (\dot{A} | Q \frac{i}{z - QLQ} Q | \dot{A}). \quad (29)$$

The extension to  $n$  dynamic variables, where Eq. (28) is an equation of the  $n \times n$  Green's functions, is

$$G^+(z) = -a(za - \omega + iF)^{-1}(-\omega + iF), \quad (30)$$

where

$$a_{ij} = (A_i | A_j), \quad (31)$$

$$\omega_{ij} = (A_i | L | A_j) = -i(\dot{A}_i | A_j), \quad (32)$$

$$F_{ij} = (\dot{A}_i | Q \frac{i}{z - QLQ} Q | \dot{A}_j), \quad (33)$$

$$P = \sum_{ij} |A_i\rangle (a^{-1})_{ij} \langle A_j|, \quad Q = 1 - P. \quad (34)$$

In the following, we shall consider

$$X(\vec{q}), \quad \dot{X}(\vec{q}), \quad \mathcal{H}(\vec{q}), \quad \dot{\mathcal{H}}(\vec{q}), \quad (35)$$

as dynamic variables.  $X(\vec{q})$  and  $\dot{X}(\vec{q})$  are closely related to  $\rho(\vec{q})$  and  $\dot{\rho}(\vec{q})$ , respectively, because they represent the first term in an expansion with respect to  $\vec{q}$ . The conserved variable  $\mathcal{H}$  must be included to account for heat-conduction phenomena. Moreover, the order-parameter and energy fluctuations are coupled below  $T_c$ , because  $\langle X(-\vec{q}) \mathcal{H}(\vec{q}) \rangle$  and  $\langle \dot{X}(-\vec{q}) \dot{\mathcal{H}}(\vec{q}) \rangle$  do not vanish below  $T_c$ . In fact, from Eqs. (5), (7), (8), and (19), it follows that

$$\begin{aligned}
\langle X(-\vec{q})\mathcal{K}(\vec{q}) \rangle &= B(\langle X \rangle^3 - \langle X^3 \rangle) \langle X(-\vec{q})X(\vec{q}) \rangle + 2C[F(\vec{0}) - F(\vec{q})] \langle X \rangle \langle X(-\vec{q})X(\vec{q}) \rangle \\
&+ \frac{1}{2} \frac{1}{N^{1/2}} \sum_{\vec{q}} [A + 3B \langle X \rangle^2 - 4CF(\vec{q}')] \langle X(-\vec{q})X(\vec{q}')X(\vec{q} - \vec{q}') \rangle \\
&+ B \langle X \rangle \frac{1}{N} \sum_{\vec{q}_1, \vec{q}_2} \langle X(-\vec{q})X(\vec{q}_1)X(\vec{q}_2)X(\vec{q} - \vec{q}_1 - \vec{q}_2) \rangle \\
&+ \frac{B}{4} \frac{1}{N^{3/2}} \sum_{\vec{q}_1, \vec{q}_2, \vec{q}_3} \langle X(-\vec{q})X(\vec{q}_1)X(\vec{q}_2)X(\vec{q}_3)X(\vec{q} - \vec{q}_1 - \vec{q}_2 - \vec{q}_3) \rangle, \tag{36}
\end{aligned}$$

$$\langle X(\vec{0})\mathcal{K}(\vec{0}) \rangle = k_B T^2 \frac{d\langle X \rangle}{dT}, \tag{37}$$

$$\langle \dot{X}(-\vec{q})\dot{\mathcal{K}}(\vec{q}) \rangle = 2C \langle X \rangle [F(\vec{0}) - F(\vec{q})] \frac{k_B T}{M}. \tag{38}$$

Here we took the classical limit of the scalar products defined by Eq. (23), namely,

$$(A|B) = \int_0^\beta d\lambda \langle e^{\lambda\mathcal{K}} A^\dagger e^{-\lambda\mathcal{K}} B \rangle = \beta \langle A^\dagger B \rangle. \tag{39}$$

From the expressions, it is seen that below  $T_c$ , order parameter and energy fluctuations do couple. As a consequence, heat-conduction phenomena are expected to occur not only in  $\hat{G}_{xx}^*$  but also in  $\hat{G}_{xx}^*$ , below  $T_c$ .

For completeness we also list

$$\langle \dot{X}(-\vec{q})\dot{X}(\vec{q}) \rangle = k_B T/M, \tag{40}$$

$$\begin{aligned}
M \langle \ddot{X}(-\vec{q})\ddot{X}(\vec{q}) \rangle / \langle \dot{X}(\vec{q})\dot{X}(-\vec{q}) \rangle &= A - 12C + 3B \langle X^2 \rangle \\
&+ 4C[F(\vec{0}) - F(\vec{q})] \\
&= M\omega_A^2(\vec{q}), \tag{41}
\end{aligned}$$

$$\begin{aligned}
\langle \dot{\mathcal{K}}(-\vec{q})\dot{\mathcal{K}}(\vec{q}) \rangle &= 4C \frac{k_B T}{M} \langle X \rangle^2 [F(\vec{0}) - F(\vec{q})]^2 \\
&+ \frac{4C^2}{M} k_B T \frac{1}{N} \sum_{\vec{q}'} [|\langle X(\vec{q} - \vec{q}') \rangle|^2] \\
&+ \langle |X(\vec{q}')|^2 \rangle [F^2(\vec{q}') - F(\vec{q}')F(\vec{q}' - \vec{q})], \tag{42}
\end{aligned}$$

which follow from Eqs. (11) and (19).

### C. Excitation spectrum

Before turning to examine the explicit results, it is helpful to summarize those features of the excitation spectrum that might be expected on general grounds. At low temperatures, the particles oscillate about a mean position determined by the order parameter. The displacements are small and anharmonic perturbation theory is adequate. We therefore expect an excitation spectrum exhibiting phonons and, by virtue of energy conservation, heat diffusion or second-sound modes. The resulting Rayleigh peak or second-sound peaks

may occur in both the energy and displacement Green's functions, due to the coupling between order-parameter and energy fluctuations below  $T_c$ .

With increasing temperature, anharmonic effects become more significant, and large-amplitude oscillations will appear, because the particles can overcome the potential barrier. Experience with the corresponding two-dimensional systems, which we studied previously, suggests that this will result in the formation and dynamics of clusters.<sup>5,6</sup> A cluster represents particles connected by nearest-neighbor bonds, having displacements with a sign opposite to that expected from zero temperature. A cluster is surrounded by a cluster wall where the displacements  $X_i$  change sign. This phenomenon illustrates the importance of the solitary kink solution of the underlying equation of motion in the continuous limit.<sup>15,16</sup> One anticipates, on the basis of the two-dimensional systems, that the formation and dynamics of the clusters will certainly affect the excitation spectrum producing, in particular, a central peak.<sup>5,6</sup> This peak will be superimposed, at least below  $T_c$ , on the heat-diffusion peak. In this temperature domain (immediately below  $T_c$ ), second sound is unlikely due to the effectively strong anharmonicity. A collective excitation in the energy fluctuations can be expected only in a temperature window below  $T_c$ . The lower limit is reached when anharmonicity is too small to allow a collective excitation; at the upper limit, second sound becomes overdamped and changes over to heat diffusion, due to anharmonicity.

Above  $T_c$ , order-parameter and energy fluctuations are no longer coupled. Hence, heat diffusion will appear only in the energy Green's function. Nevertheless, a central peak will be expected in the displacement spectral density due to the cluster dynamics.

Of course, the optical-phonon branch will also exhibit a strong temperature dependence, becoming soft (for small wave vectors) in the vicinity of  $T_c$ . Above  $T_c$ , where the coupling between order parameter and energy vanishes, the phonon res-

onance will appear only in the displacement Green's function.

Finally, at very high temperatures, the oscillators will be nearly independent. Hence, the spectrum is expected to be close to that of a quartic anharmonic oscillator.

Next, we substantiate these conjectures by studying the excitation spectrum in several limits. We consider the high-frequency approximation, the low-frequency, low-temperature approximation, the implications of large-amplitude oscillations, and, finally, nonlinear heat-pulse propagation. We shall find that the results of this analysis amplify the interpretation of the numerical results.

### 1. High-frequency approximation

In a first step, we consider only  $X(\bar{q})$  and  $\dot{X}(\bar{q})$  explicitly. According to Eqs. (30)–(34), we obtain for the order parameter, Green's function

$$G_{xx}^*(\bar{q}, z) = -\omega_T^2 \langle X(-\bar{q})X(\bar{q}) \rangle \times [z^2 + iz(M/k_B T)F_{\dot{x}\dot{x}}(\bar{q}, z) + \omega_T^2]^{-1}, \quad (43)$$

where

$$\omega_T^2 = k_B T / \langle X(-\bar{q})X(\bar{q}) \rangle, \quad (44)$$

$$F_{\dot{x}\dot{x}}(\bar{q}, z) = \langle \dot{X}(-\bar{q}) | Q \frac{i}{z - QLQ} Q | \dot{X}(\bar{q}) \rangle,$$

$$Q = 1 - P, \quad P = |X\rangle \frac{1}{\langle X|X\rangle} \langle X| + |\dot{X}\rangle \frac{1}{\langle \dot{X}|\dot{X}\rangle} \langle \dot{X}|. \quad (45)$$

To study the regularity of  $F_{\dot{x}\dot{x}}(\bar{q}, z)$ , we rewrite Eq. (44) in the form

$$F_{\dot{x}\dot{x}} = \langle \dot{X}_1 | [i/(z - L_1)] \dot{X}_1 \rangle, \quad (46)$$

where

$$\dot{X}_1 = Q\dot{X}, \quad L_1 = QLQ, \quad (47)$$

and introduce the projector

$$P_1 = [\dot{X}_1] \langle \dot{X}_1^\dagger \dot{X}_1 \rangle^{-1} \langle \dot{X}_1 |, \quad (48)$$

so that

$$F_{\dot{x}\dot{x}} = \frac{i \langle \dot{X}_1^\dagger \dot{X}_1 \rangle}{z + iF_{11} / \langle \dot{X}_1^\dagger \dot{X}_1 \rangle}, \quad (49)$$

where

$$F_{11} = \langle Q_1 iL_1 \dot{X}_1^\dagger [i/(z - Q_1 L_1 Q_1)] Q_1 iL_1 \dot{X}_1 \rangle, \quad (50)$$

$$\langle \dot{X}_1^\dagger \dot{X}_1 \rangle = \omega_A^2 - \omega_T^2, \quad (51)$$

$$M\omega_A^2 = A - 12C + 3B\langle X^2 \rangle + 4C[F(\bar{0}) - F(\bar{q})]. \quad (52)$$

Substitution of relation (49) into (43) yields

$$G_{xx}^*(\bar{q}, z) = -\omega_T^2 \langle X(-\bar{q})X(\bar{q}) \rangle \times \left( z^2 - \omega_T^2 - z \frac{\omega_A^2 - \omega_T^2}{z + iF_{11} / \langle \dot{X}_1^\dagger \dot{X}_1 \rangle} \right)^{-1}. \quad (53)$$

The regularity of  $F_{11}(\bar{q}, z)$  in  $z$  will be affected by strong anharmonicity and for small  $z$  by the heat-conduction pole. At high frequencies and low temperatures, we expect, therefore, a weakly damped phonon resonance at

$$z = \pm \omega_A, \quad (54)$$

where  $\omega_A$  is given by Eq. (52).

### 2. Small-frequency low-temperature approximation

At low temperature ( $T \ll T_c$ ), the low-frequency spectrum will be affected by heat diffusion or second sound and the coupling between order-parameter and energy fluctuations. To allow the possibility of second sound, we have to consider four variables, namely,  $X(\bar{q})$ ,  $\dot{X}(\bar{q})$ ,  $\mathcal{X}(\bar{q})$ , and  $\dot{\mathcal{X}}(\bar{q})$ . To simplify the discussion, we ignore the memory function matrix. Accordingly, we assume that second sound is a well-defined excitation. In this case, the Green's function matrix is, according to Eq. (30),

$$G^*(\bar{q}, z) = a(za - \omega)^{-1}\omega = (z - \omega a^{-1})^{-1}\omega. \quad (55)$$

The matrices  $a$  and  $\omega$  are

$$a = \begin{bmatrix} a_{11} & a_{12} & 0 & 0 \\ a_{21} & a_{22} & 0 & 0 \\ 0 & 0 & a_{33} & a_{34} \\ 0 & 0 & a_{43} & a_{44} \end{bmatrix} \quad (56)$$

$$\omega = \begin{bmatrix} 0 & 0 & ia_{33} & ia_{34} \\ 0 & 0 & ia_{43} & ia_{44} \\ -ia_{33} & -ia_{34} & 0 & 0 \\ -ia_{43} & -ia_{44} & 0 & 0 \end{bmatrix}, \quad (57)$$

where

$$\begin{aligned} a_{11} &= \langle X(-\bar{q})X(\bar{q}) \rangle, \\ a_{12} &= \langle X(-\bar{q})\mathcal{X}(\bar{q}) \rangle, \\ a_{33} &= \langle \dot{X}(-\bar{q})\dot{X}(\bar{q}) \rangle = k_B T / M, \\ a_{34} &= \langle \dot{X}(-\bar{q})\dot{\mathcal{X}}(\bar{q}) \rangle, \\ a_{22} &= \langle \mathcal{X}(-\bar{q})\mathcal{X}(\bar{q}) \rangle, \\ a_{44} &= \langle \dot{\mathcal{X}}(-\bar{q})\dot{\mathcal{X}}(\bar{q}) \rangle. \end{aligned} \quad (58)$$

The relevant Green's functions can now be calculated by matrix algebra. This leads to the following expressions:

$$G_{11} = G_{xx} = \frac{(z^2 - L_{42})a_{33} - a_{43}L_{32}}{(z^2 - L_{31})(z^2 - L_{42}) + L_{41}L_{32}}, \quad (59)$$

$$G_{22} = G_{\mathcal{X}\mathcal{X}} = \frac{a_{44}(z^2 - L_{31}) + a_{34}L_{41}}{(z^2 - L_{31})(z^2 - L_{42}) + L_{41}L_{32}}, \quad (60)$$

where

$$\begin{aligned} L_{31} &= (1/b)(a_{33}a_{22} - a_{34}a_{21}), \\ L_{41} &= (1/b)(a_{43}a_{22} - a_{44}a_{21}), \end{aligned} \quad (61)$$

$$\begin{aligned} L_{32} &= (1/b)(a_{33}a_{12} - a_{34}a_{11}), \\ L_{42} &= (1/b)(a_{43}a_{12} - a_{44}a_{11}), \\ b &= a_{11}a_{22} - a_{12}a_{21}. \end{aligned} \quad (62)$$

The poles are given by

$$z^2 = \frac{1}{2}[L_{31} + L_{42} \pm \{(L_{31} + L_{42})^2 - 4(L_{31}L_{42} + L_{41}L_{32})\}^{1/2}], \quad (63)$$

where  $z_+$  describes the optical-phonon branch and  $z_-$  the second sound. The crucial feature is that second sound will appear in both  $\hat{G}_{xx}$  and  $\hat{G}_{\mathcal{J}\mathcal{C}\mathcal{J}\mathcal{C}}$ , provided that the coupling between order-parameter and energy fluctuations ( $a_{12}, a_{34}$ ) does not vanish. In fact, if we set  $a_{12} = a_{34} = 0$ , the Green's functions (59) and (60) reduce to

$$G_{11} = \frac{a_{33}}{z^2 - a_{33}/a_{11}}, \quad G_{22} = \frac{a_{44}}{z^2 - a_{44}/a_{22}}. \quad (64)$$

From the  $q$  dependence of terms entering the second-sound frequency  $z_-$  [Eq. (63)], we find for the second-sound velocity, the relation

$$\begin{aligned} C_{ss}^2 &= \frac{1}{a_{22}(\bar{q} = \bar{0})} \frac{4C^2 k_B T}{M} \lim_{\bar{q} \rightarrow 0} \frac{1}{q^2} \frac{1}{N} \\ &\times \sum_{\bar{q}'} [ \langle |X(\bar{q} - \bar{q}')|^2 \rangle + \langle |X(\bar{q}')|^2 \rangle ] \\ &\times [ F(\bar{q}') - F(\bar{q}')F(\bar{q}' - \bar{q}) ]. \end{aligned} \quad (65)$$

An estimate may be obtained by setting

$$\langle |X(\bar{q} - \bar{q}')|^2 \rangle + \langle |X(\bar{q}')|^2 \rangle \approx 2k_B T / M\omega_A^2(\bar{0}), \quad (66)$$

where the phonon frequency is given by Eq. (52). This approximation is reasonable because at low temperatures,  $\langle |X(\bar{q})|^2 \rangle$  is dominated by the phonon resonance, having small dispersion. Substituting Eq. (66) into (65) and expanding  $F(\bar{q}' - \bar{q})$  for small  $\bar{q}$ , we find

$$C_{ss}^2 = \frac{2C^2(k_B T)^2 a^2}{\langle \mathcal{J}\mathcal{C}(\bar{0})\mathcal{J}\mathcal{C}(\bar{0}) \rangle M\omega_A^2(\bar{0})} \approx \frac{2C^2 a^2}{M\omega_A^2(\bar{0})}. \quad (67)$$

In the last step we used

$$\langle \delta\mathcal{J}\mathcal{C} \delta\mathcal{J}\mathcal{C} \rangle = \langle \mathcal{J}\mathcal{C}(\bar{0})\mathcal{J}\mathcal{C}(\bar{0}) \rangle = k_B T^2 \frac{d\langle \mathcal{J}\mathcal{C} \rangle}{dT} \quad (68)$$

and

$$\langle \mathcal{J}\mathcal{C} \rangle = k_B T + \langle \mathcal{J}\mathcal{C} \rangle_{T=0}, \quad (69)$$

which holds at low temperatures.

For the optical-phonon frequency, we obtain from Eq. (63) at  $\bar{q} = \bar{0}$ ,

$$\begin{aligned} z_+^2 &= \frac{a_{33}}{a_{11}} \left( 1 - \frac{a_{12}a_{21}}{a_{11}a_{12}} \right)^{-1} \\ &= \omega_T^2(0) \left( 1 - \frac{\langle \delta X \delta \mathcal{J}\mathcal{C} \rangle^2}{\langle \delta X \delta X \rangle \langle \delta \mathcal{J}\mathcal{C} \delta \mathcal{J}\mathcal{C} \rangle} \right)^{-1}, \end{aligned} \quad (70)$$

where

$$\omega_T^2 = k_B T / \langle X(\bar{0})X(\bar{0}) \rangle = k_B T / \langle \delta X \delta X \rangle, \quad (71)$$

$$\langle \delta X \delta \mathcal{J}\mathcal{C} \rangle = \langle X(\bar{0})\mathcal{J}\mathcal{C}(\bar{0}) \rangle = k_B T^2 \frac{d\langle X \rangle}{dT}, \quad (72)$$

$$\langle \delta \mathcal{J}\mathcal{C} \delta \mathcal{J}\mathcal{C} \rangle = \langle \mathcal{J}\mathcal{C}(\bar{0})\mathcal{J}\mathcal{C}(\bar{0}) \rangle = k_B T^2 \frac{d\langle \mathcal{J}\mathcal{C} \rangle}{dT}.$$

These estimates are expected to describe the essential features of the excitation spectrum in a temperature window below  $T_c$ . In fact, second sound can occur only if anharmonicity is sufficiently strong, allowing a propagating collective mode of the energy density.<sup>11,12</sup>

At very low temperatures, anharmonicity and the coupling between energy and order-parameter fluctuations becomes very small. At zero temperature, where  $a_{12} = a_{34} = 0$ ,  $G_{11} = G_{xx}$  reduces to [Eq. (64)]

$$\frac{G_{xx}(\bar{q}, z)}{a_{11}(\bar{q})} = \frac{a_{33}}{a_{11}} \frac{1}{z^2 - a_{33}/a_{11}} = \omega_A^2 \frac{1}{z^2 - \omega_A^2}, \quad (73)$$

where, according to Eq. (52),

$$M\omega_A^2 = 2(12C - A) + 4C[F(\bar{0}) - F(\bar{q})], \quad (74)$$

because

$$\langle X^2 \rangle_{T=0} = (12C - A)/B. \quad (75)$$

However,  $G_{22} = G_{\mathcal{J}\mathcal{C}\mathcal{J}\mathcal{C}}$  will not reduce to the simple expression listed in Eq. (64) because anharmonicity becomes so small that second sound cannot occur. Here, the structure of  $G_{22}$  can be determined from the equation of motion for  $\mathcal{J}\mathcal{C}(q)$  [Eq. (19)]. At very low temperatures, the second term will dominate so that at  $T = 0$ ,

$$\frac{G_{\mathcal{J}\mathcal{C}\mathcal{J}\mathcal{C}}(\bar{q}, z)}{a_{22}(\bar{q})} = \omega_A^2 \frac{1}{z^2 - \omega_A^2} = \frac{G_{xx}(\bar{q}, z)}{a_{11}(\bar{q})}. \quad (76)$$

For very small but finite  $T$ , the first term in Eq. (19) will give rise to an additional structure for small  $z$ , due to two phonon processes.

At the upper limit of the window, second sound ceases to be a well-defined excitation due to the strong anharmonicity. It will become overdamped and gradually change over to diffuse heat conduction.

### 3. Large-amplitude oscillations

So far, we have only discussed the small-amplitude oscillation regime, where almost all particles will sit in the left or right well of

$$\frac{1}{2}(A - 12C)X^2 + \frac{1}{4}BX^4 = V(X), \quad (77)$$

depending on the preparation of the low-temperature phase. As soon as the temperature becomes larger or comparable to the depth of the well

$$V[X^2 = (12C - A)/B] = -\frac{1}{4}(12C - A)^2/B, \quad (78)$$

the particles will also undergo large-amplitude oscillations, which can no longer be described by conventional phonon-perturbation theory. For the model parameters listed in Eq. (2), the temperature corresponding to the depth of the well is  $k_B T = 6.75$ .

To illustrate the implications of those points, we consider (following Krumhansl and Schrieffer<sup>15</sup>) the equation of motion in the continuum limit. Denoting the total displacement field by  $g(\vec{X})$ , the equation of motion corresponding to Hamiltonian (1) reads for  $\vec{X} = (X, 0, 0)$ ,

$$-M\ddot{g}(X) = (A - 12c)g + Bg^3 - 2Ca^2g_{xx}, \quad (79)$$

having the solitary wave solution

$$g(X, t) = g(X - vt) = \left(\frac{12C - A}{B}\right)^{1/2} \tanh\left(\frac{X - vt}{\xi 2^{1/2}}\right), \quad (80)$$

where

$$\xi^2 = (2Ca^2 - v^2M)/(12C - A). \quad (81)$$

According to this kink solution, the displacement field is constant over the semi-infinite region  $X - vt < 0$  and given by the negative value of the zero-temperature parameter [Eq. (3)]. For  $X - vt > 0$ , however, the displacement field equals the positive value of the zero-temperature order parameter. The transition takes place through a cluster wall of approximate thickness  $2\sqrt{2}\xi$ , and the wall moves with velocity  $v$ .

From our work on the two-dimensional version of the present model, we know that the kink solution is relevant to the explanation of the formation and the dynamics of clusters.<sup>5,6</sup> A cluster represents particles connected by a nearest-neighbor bond and having a local displacement with a sign opposite to the zero-temperature order parameter. Different clusters are separated by cluster walls, where the local displacement changes sign, in close analogy to the above kink solution. It should be borne in mind, however, that the formation of clusters and their dynamics will set in gradually with increasing temperature. In fact, particles have to overcome the potential barrier to form a cluster. At very high temperatures, on the other hand, the system will behave like independent quartic oscillators, so that the dispersion term in Eq. (79) can be ignored. Consequently, one anticipates that the kink solution will then no

longer play a significant role in the statistical mechanics.

#### D. Nonlinear heat-pulse propagation

Heat-pulse techniques have been used extensively in the past to study second sound.<sup>17</sup> Experimentally, the systems are usually studied at very low temperatures, where the available power input is insufficient to drive the nonlinearities. In this regime, the propagation of heat can be described by a diffusion or wave equation, or in other words, within the framework of linear response theory.

In this section, we study the possibility of nonlinear heat propagation. In doing so, we consider the effect of the nonlinearities on the phononlike solutions. It is convenient to recast the equation of motion (11) in the continuum approximation

$$\begin{aligned} -M\ddot{f}(\vec{R}, t) = & \langle X \rangle (A - 12C + B\langle X \rangle^2) \\ & + (A - 12C + 3B\langle X \rangle^2)f + 3B\langle X \rangle f^2 \\ & + Bf^3 - 2Ca^2\nabla^2 f, \end{aligned} \quad (82)$$

where  $f(\vec{R}, t)$  denotes the fluctuating part of the displacement field. We wish to consider solutions which reduce to phonons. For this purpose we follow Varma<sup>16</sup> and introduce a small parameter  $\epsilon$  so that for  $\epsilon = 0$ , we have a linear problem. The equation of motion is then

$$\begin{aligned} -M\ddot{f} = & \langle X \rangle (A - 12C + B\langle X \rangle^2) + (A - 12C + 3B\langle X \rangle^2)f \\ & + 3\epsilon B\langle X \rangle f^2 + B\epsilon^2 f^3 - 2C\nabla^2 f. \end{aligned} \quad (83)$$

Following Varma we look for solutions which reduce to phonons in the linear limit. Restricting the analysis to one space dimension, we set

$$\begin{aligned} f(x, t) = & [\varphi^{(0)}(X, T) + \tilde{\varphi}^{(0)}(X, T)]\epsilon \\ & + \sum_{\substack{n=1 \\ n \neq 0}}^{n=\infty} \varphi^{(n)}(X, T)\epsilon^{|n|-1} e^{in(qx - \omega_0 t)}. \end{aligned} \quad (84)$$

It is assumed that the variations in  $\varphi^{(1)}(X, T)$  are slow compared to the phonon part. Accordingly, we introduce, following Varma,<sup>16</sup>

$$T = \epsilon t, \quad X = \epsilon x. \quad (85)$$

Equation (83) then becomes

$$\begin{aligned} f_t - 2Ca^2 f_{xx} - A_2 f + 3\epsilon B\langle X \rangle f^2 + \epsilon^2 B f^3 + \epsilon^2 f_{TT} \\ - 2C\epsilon^2 f_{XX} + 2\epsilon f_{tT} - 4\epsilon C a^2 f_{xx} = 0, \end{aligned} \quad (86)$$

where

$$A_2 = 12C - A - 3B\langle X \rangle^2. \quad (87)$$

We have assumed that

$$12C - A - B\langle X \rangle^2 \approx 0, \quad (88)$$

which holds for very low temperatures [see Eq.

(3)].

Inserting (84) into (86), equating dc first and second harmonic terms, we get

$$\varphi^{(0)} = 3 \frac{B\langle X \rangle}{A_2} |\varphi^{(1)}|^2, \quad \varphi^{(2)} = \frac{B\langle X \rangle}{A_2} (\varphi^{(1)})^2 \quad (89)$$

and

$$(-2i\omega_0\varphi_T^{(1)} - 4iqCa^2\varphi^{(1)}) + \epsilon \frac{42B\langle X \rangle}{A_2} + 3B \\ \times |\varphi^{(1)}|^2\varphi^{(1)} + \varphi_{TT}^{(1)} - 2Ca^2\varphi_{XX}^{(1)} = 0. \quad (90)$$

Introducing the group velocity

$$V_G = \frac{d\omega_0}{dk} = \frac{2Ca^2q^2}{\omega_0}, \quad (91) \\ \omega_0^2 = (A - 12C + 3B\langle X \rangle^2) + 2Ca^2q^2,$$

and the new scales

$$z = X - V_G T, \quad s = \epsilon T, \quad (92)$$

Equation (90) reduces in lowest order in  $\epsilon$  to the nonlinear Schrödinger equation<sup>18,19</sup> (NLS)

$$i\varphi_s^{(1)} + P\varphi_{zz}^{(1)} + R|\varphi^{(1)}|^2\varphi^{(1)} = 0, \quad (93)$$

where

$$P = \frac{2Ca^2 - V_G^2}{2\omega_0}, \quad R = -\frac{B}{2\omega_0} \left( 3 + \frac{42\langle X \rangle^2}{A_2} \right). \quad (94)$$

The solution of the NLS equation depends in a crucial way on the sign of  $PR$ . Here  $PR$  is negative. In this case, one class of stable solutions is plane waves with frequency

$$\omega = PR^2 - R. \quad (95)$$

Other stable solutions can be obtained by noting that for  $PR < 0$  the NLS can be reduced to the Korteweg-de Vries (KdV) equation. This can be achieved by following the procedure of Taniuti and Yajima.<sup>20</sup> One introduces real functions  $\rho$  and  $\sigma$  by

$$\varphi^{(1)} = \rho^{1/2} \exp i \int_0^z \frac{\sigma}{2\rho} dz'. \quad (96)$$

Substituting (96) into (93) and separating real and imaginary parts, one finds

$$\rho_s + (\rho\sigma)_z = 0, \\ \sigma_s + \sigma\sigma_z = 2PR\rho_z + P^2[\rho^{-1/2}(\rho^{-1/2}\rho_z)]_z. \quad (97)$$

Now one introduces the small parameter  $\mu$  and writes

$$\rho = \rho_0 + \mu\rho_1 + \dots, \\ \sigma = \sigma_0 + \mu\sigma_1 + \dots, \quad (98)$$

and also introduces new scales

$$z' = \mu^{1/2}(z - \gamma s), \quad s' = \mu^{3/2}s. \quad (99)$$

Carrying out the asymptotic analysis, one finds

$$\gamma = \sigma_0 + (2|PR|\rho_0)^{1/2}, \\ \rho_1(z', s') = -\left(\frac{2|PR|}{\rho_0}\right)^{1/2} \sigma_1(z', s'), \quad (100)$$

where  $\sigma_1$  obeys the KdV equation

$$\sigma_{1s'} + \sigma_1\sigma_{1z'} + \delta^2\sigma_{1z'z'} = 0, \quad (101)$$

with

$$\delta^2 = (P^2/\rho_0)(2|PR|/\rho_0)^{-1/2}. \quad (102)$$

A soliton solution of the KdV equation (101) is<sup>18,19</sup>

$$\sigma_1 = 2u \operatorname{sech}^2\left(\frac{\sqrt{u}}{2} \frac{z' - us'}{\delta}\right) = \sigma_1(z' - us'). \quad (103)$$

From our point of view, the important result is that the effect of the nonlinearities on the phonon-like solutions leads to a modulation of the amplitude. In the lowest order of asymptotic expansions, the original equation was reduced to the KdV equation, which exhibits solitons, determining the amplitude modulation. One expects, therefore, that the effect of the nonlinearities on the phononlike solutions will lead to an envelope or modulation of plane waves, in terms of envelope solitons.<sup>21</sup>

In general, solitons have certain features in common.<sup>18,19</sup> These mutual features are (i) an initial perturbation can break up into a series of solitons; (ii) solitons may collide and pass through each other without change of shape or velocity but with a phase shift; and (iii) the speed of an individual soliton often depends on its amplitude.

The first property implies that a heat pulse representing an initial perturbation of our system can break up into envelope solitons. In our case, the heat pulse can be described by the kinetic energy, describing the temperature field

$$k_B T(X, t) = Mf(X, t)^2. \quad (104)$$

From Eqs. (84), (89), (96), (98), (103), and (104), we find that the height  $H$  of the envelope soliton is proportional to the third power of its velocity

$$H \sim u^3, \quad (105)$$

and its half-width  $\Delta$  obeys

$$\Delta \sim u^{-1/2}, \quad (106)$$

so that

$$\Delta \sim H^{-1/6}. \quad (107)$$

This analysis indicates that nonlinear heat conduction might be associated with envelope solitons, provided that the effects of nonlinearity are sufficiently small. It should be remembered, how-

ever, that the foregoing analysis is somewhat oversimplified in that we have considered only a one-dimensional system in the continuum approximation.

### III. MOLECULAR-DYNAMICS TECHNIQUE

To simulate a canonical ensemble, we assume that the particles suffer collisions with much lighter ones, which represent the heat bath. The collisions are described by a friction  $-\Gamma p_i$  and a random force  $\eta_i(t)$ . The associated equations of motion are then coupled Langevin equations

$$M\ddot{X}_i = -\delta\mathcal{H}/\delta X_i - \Gamma M\dot{X}_i + \eta_i(t), \quad (108)$$

where

$$\langle \eta_i(t)\eta_{i'}(t') \rangle = 2M\Gamma k_B T \delta_{ii'} \delta(t-t'). \quad (109)$$

$T$  denotes the temperature of the bath. The stationary solution of the associated Fokker-Planck equation is the canonical distribution

$$p_{\text{eq}}(\dot{X}_1, \dots, \dot{X}_N; X_1, \dots, X_N) \sim e^{-\beta\mathcal{H}}. \quad (110)$$

Starting from initial values for positions and velocities, the particles are then allowed to move under the influence of the computer-generated random force. The temporal evolutions of the variables are then calculated with a set of difference equations approximating the Langevin equations (110). On this basis, one obtains

$$X_i(t), \dot{X}_i(t), \ddot{X}_i(t), \dots, \text{etc.}$$

For a more detailed description of the algorithm and the random force generation, we refer the reader to the Appendix.

The system is then allowed to age or, in other words, to reach equilibrium. After this interval, the subsequent  $10^5$  steps are used to perform time average, representing estimates for canonical ensemble averages. An example is

$$\langle X \rangle = \left\langle \frac{1}{N} \sum_i X_i \right\rangle \approx \frac{1}{\tau} \int_0^\tau \left( \frac{1}{N} \sum_i X_i(t) \right) dt. \quad (111)$$

It is obvious that the dynamic properties will be modified, in particular due to the damping term in Eq. (108). To reduce these modifications  $\Gamma$  must be chosen in such a way that

$$1/\Gamma \gg \tau_c, \quad (112)$$

where  $\tau_c$  denotes the characteristic times of the dynamics. This implies, for example, that the excitations do not become overdamped due to the friction term. Another important constraint on  $\Gamma$  evolves from the energy conservation of a Hamiltonian system. Since our system evolves according to the Langevin equations, we obtain from Eq. (108),

$$\begin{aligned} \frac{d\mathcal{H}}{dt} &= \sum_i \left( \frac{\delta\mathcal{H}}{\delta p_i} \frac{\delta p_i}{\delta t} + \frac{\delta\mathcal{H}}{\delta X_i} \frac{\delta X_i}{\delta t} \right) \\ &= - \sum_i [\Gamma M \dot{X}_i^2 - \dot{X}_i \eta_i(t)]. \end{aligned} \quad (113)$$

Consequently, energy is not conserved because the Hamiltonian system is in contact with the heat bath. To avoid artificial features due to the random-noise pulses, the mean time between two pulses must be small compared to  $\tau_c$ . In this case, we may average Eq. (113) over some pulses. This leads to the expression

$$\begin{aligned} \frac{d\mathcal{H}}{dt} &= -\Gamma \sum_i [M \dot{X}_i^2(t) - k_B T] \\ &= -\Gamma [2E_k(t) - Nk_B T], \end{aligned} \quad (114)$$

implying that energy is nearly conserved in the time interval  $\tau_c$ ,

$$1/\Gamma \gg \tau_c, \quad (115)$$

which is equivalent to Eq. (112). Since the system evolves according to the Langevin equation, the time interval over which its evolution is followed must clearly be larger than  $1/\Gamma$ , so that

$$1/\Gamma \gg \tau_{\text{ch}}. \quad (116)$$

$\tau_{\text{ch}}$  denotes the equilibrium chain length. Combining Eqs. (112) and (116), we finally obtain

$$\tau_{\text{ch}} \gg 1/\Gamma \gg \tau_c. \quad (117)$$

From this relation, it becomes evident that energy can be nearly conserved provided that  $\Gamma$  and the chain length  $\tau_{\text{ch}}$  are appropriately chosen. An exception is the region very close to  $T_c$ , where the characteristic times become very long. In this region, however, numerical methods become difficult in any case because the linear dimension of the system must exceed the correlation length, to avoid finite size effects.

To summarize this section, the above molecular-dynamics technique allows the simulation of the canonical ensemble where the global temperature is fixed. Energy conservation can be nearly realized by choosing the damping constant  $\Gamma$  appropriately. The numerical solution of the coupled Langevin equations then allows estimates of all the static and dynamic properties which can be derived from the variables entering the Hamiltonian. This includes static and dynamic properties. For a detailed discussion of the algorithm and the calculation of time-dependent correlation functions, we refer to the Appendix and Ref. 22, respectively.

### IV. NUMERICAL RESULTS

In this section, we present and discuss some numerical results as obtained with the molecular-

dynamics technique described in Sec. III, and applied to systems of  $10^3$  and  $8 \times 10^3$  particles, subjected to periodic boundary conditions.

#### A. Static properties

The partition function associated with Hamiltonian (1) reduces in the limit as  $A \rightarrow -\infty$ ,  $B \rightarrow +\infty$ , but  $A/B = -1$ , to that of the Ising ferromagnet.<sup>3</sup> Invoking the universality hypothesis, one therefore expects that the static critical exponents should be equal to the three-dimensional spin- $\frac{1}{2}$  Ising model, except at the displacive limit ( $12C = A$ ), representing an isolated point.<sup>14</sup> In this case, it makes sense to plot the order parameter as a function of  $T$  to the power  $\frac{16}{5}$  and the isothermal susceptibility as  $\chi_T^{-4/5}$ , anticipating three-dimensional Ising-model behavior<sup>20</sup>

$$\langle X \rangle = G(T_c - T)^{16/5}, \quad (118)$$

$$\chi_T = \Gamma^\pm |T_c - T|^{-5/4}. \quad (119)$$

In Fig. 1 we summarized the calculated temperature dependence of the order parameter. From the  $\langle X \rangle^{16/5}$  plot, it is seen that the numerical estimates are consistent with the Ising power law.

Figure 2 shows the calculated temperature dependence of the isothermal susceptibility

$$\chi_T = \frac{1}{N} \sum_{i,i'} \langle \delta X_i \delta X_{i'} \rangle. \quad (120)$$

The data are again consistent with the Ising power law and yields for the universal amplitude ratio<sup>23</sup>

$$\Gamma^+/\Gamma^- \approx 6.3, \quad (121)$$

which should be compared with the corresponding ratio of the Ising model,

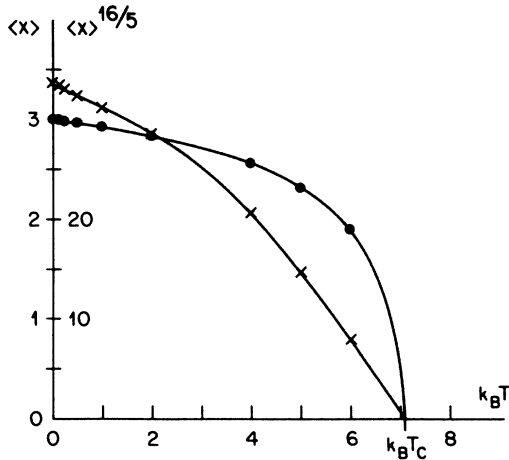


FIG. 1. Calculated temperature dependence of the order parameter  $\langle X \rangle$  and  $\langle X \rangle^{16/5}$ .

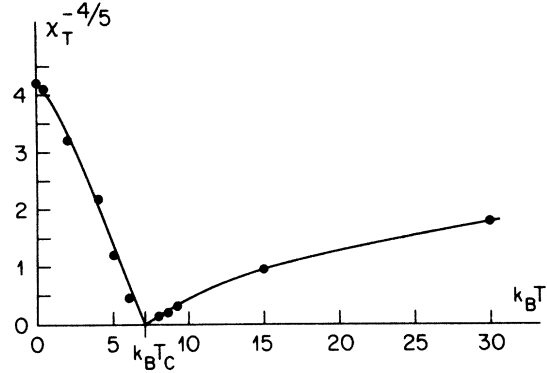


FIG. 2. Calculated temperature dependence of the isothermal susceptibility  $\chi_T$  [Eq. (120)].

$$\frac{\Gamma^+}{\Gamma^-} \Big|_{\text{Ising}} \approx 5.07, \quad (122)$$

as obtained by series.<sup>24</sup> In view of our limited data, we consider the two estimates in reasonable agreement.

From the data of  $\langle X \rangle^{16/5}$  and  $\chi_T^{-4/5}$ , we also estimated the critical temperature yielding

$$k_B T_c \approx 7.1. \quad (123)$$

The temperature dependence of various other quantities are listed in Table I.

As mentioned in Sec. II C, one expects, in analogy with the previously studied two-dimensional version of the present mode, the formation of clusters.<sup>5,6</sup> Figure 3 shows snapshots of the instantaneous positions of the particles in a plane parallel to (100). Only those particles are marked where  $\text{sgn} X_i = -\text{sgn} \langle X \rangle$ . At  $k_B T = 2$ , where the probability of overcoming the potential barrier is small, clusters rarely occur, as illustrated in Fig. 3(a). With increasing temperature, the cluster formation becomes more probable and

TABLE I. Numerical estimates for  $\langle \delta \mathcal{J} \delta \mathcal{J} \rangle$ ,  $\langle \delta X \delta X \rangle$ ,  $\langle \mathcal{J} \rangle$ ,  $\langle X_i^2 \rangle$ , and  $\omega_A$  defined in Eqs. (41) and (52).

$k_B T$	$\langle \delta \mathcal{J} \delta \mathcal{J} \rangle$	$\langle \delta X \delta X \rangle$	$\langle \mathcal{J} \rangle$	$\langle X_i^2 \rangle$	$\omega_A$
0.25	0.05	0.02	-6.50	8.94	2.44
0.50	0.28	0.09	-6.25	8.87	2.42
1	0.77	0.16	-5.74	8.73	2.39
2	4.05	0.46	-4.67	8.42	2.33
4	16.59	1.43	-2.23	7.56	2.13
5	39.13	4.00	-0.76	6.93	1.98
6	95.29	16.60	+0.91	6.17	1.78
8	49.90	89.66	+4.15	4.91	1.38
8.5	50.48	54.36	+4.55	4.94	1.39
9	58.18	37.58	+4.97	5.00	1.41
15	166.35	16.19	+9.45	5.77	1.67
30	614.45	14.07	+20.35	7.49	2.12

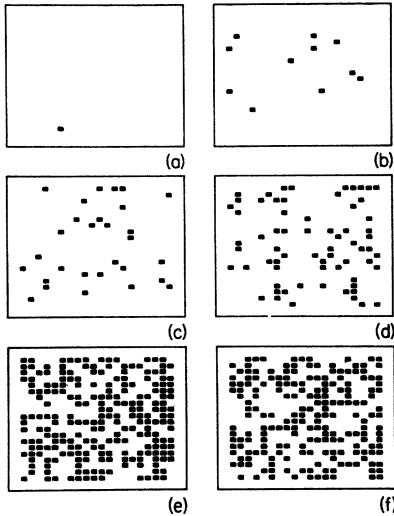


FIG. 3. Snapshots of instantaneous cluster configurations in a plane perpendicular to [100]. The squares designate particles whose local displacement  $X_i$  have a sign opposite to  $\langle X_i \rangle_{T=0}$ . (a)  $k_B T = 2$ ; (b)  $k_B T = 4$ ; (c)  $k_B T = 5$ ; (d)  $k_B T = 6$ ; (e)  $k_B T = 8$ ; (f)  $k_B T = 15$ .

the cluster size is seen to increase by approaching  $k_B T_c \approx 7.1$ . Above  $T_c$  [Figs. 3(e) and 3(f)], the clusters of positive and negative  $X_i$  must, of course, be equal on the average so that the order parameter vanishes.

The formation of these clusters and the associated cluster walls has important consequences. Their formation implies large-amplitude oscillations which can no longer be described by conventional phonon perturbation theory. The associated theoretical difficulties that beset a description of such complicated oscillations are particularly severe around  $T_c$ . In fact, at low temperatures the formation of clusters is unlikely, and at high temperatures the system will behave like uncoupled quartic oscillators. In other words, at low temperatures we have nearly linear equations with dispersion, around  $T_c$  nonlinear equations with dispersion, and at high temperatures dispersionless equations. In the present case, we know (Sec. II C) that nonlinearity and dispersion may lead to solitary waves; a prominent example is the kink solution (80), which may be interpreted as a cluster wall. Figure 3 then demonstrates that kinklike solutions play an important role around  $T_c$ , even in a discrete and three-dimensional lattice model.

### B. Dynamic properties

To investigate the excitation spectrum, we calculated the spectral densities

$$\begin{aligned} \hat{S}_{xx}(\vec{q}, \omega) &= \int_{-\infty}^{+\infty} e^{-i\omega t} \langle X(-\vec{q}, t) X(\vec{q}, 0) \rangle / \langle X(-\vec{q}, 0) X(\vec{q}, 0) \rangle \end{aligned} \quad (124)$$

and

$$\hat{S}_{\mathcal{X}\mathcal{X}}(\vec{q}, \omega) = \int_{-\infty}^{+\infty} e^{-i\omega t} \langle \mathcal{X}(-\vec{q}, t) \mathcal{X}(\vec{q}, 0) \rangle / \langle \mathcal{X}(-\vec{q}, 0) \mathcal{X}(\vec{q}, 0) \rangle, \quad (125)$$

when the variables  $X(\vec{q})$  and  $\mathcal{X}(\vec{q})$  are as defined in Eqs. (5) and (7). The Green's functions introduced in Sec. II and the spectral densities are related as follows:

$$G_{AB}^+(\omega) = \lim_{\epsilon \rightarrow 0} G_{AB}^+(z = \omega + i\epsilon) = -\chi_{AB}(\omega), \quad (126)$$

where

$$\chi_{AA}^{\parallel}(\omega) = \pi(1 - e^{-\beta\omega}) S_{AA}(\omega), \quad (127)$$

and in the classical limit,

$$\chi_{AA}^{\parallel}(\omega) = \pi\beta\omega S_{AA}(\omega). \quad (128)$$

According to Sec. II C, the excitation spectrum is expected to be rather rich and complicated due to the implications of energy conservation and the presence of small- and large-amplitude oscillations. It might be appropriate, therefore, to start with an overview of the essential features of the numerical results. In Fig. 4, we have sketched the essential features appearing in  $\hat{S}_{xx}(\vec{q}, \omega)$  and  $\hat{S}_{\mathcal{X}\mathcal{X}}(\vec{q}, \omega)$  for various temperatures at wave vectors  $\vec{q} = (0, 0, 0)$  and  $\vec{q} = (\pi/10a, 0, 0)$ , respectively. At  $k_B T = 15$  and 30, there is a broad phonon peak in  $\hat{S}_{xx}$ , but no central peak (CP) occurs.  $\hat{S}_{\mathcal{X}\mathcal{X}}$  only ex-

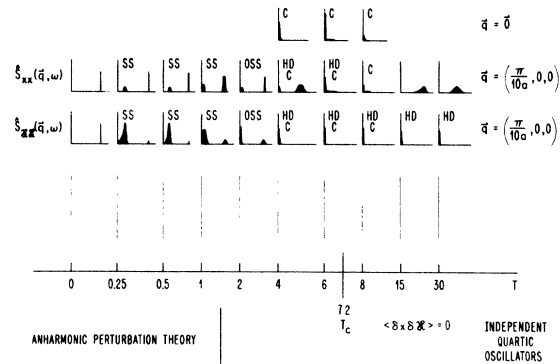


FIG. 4. Sketch of the essential features of the excitation spectrum in  $\hat{S}_{xx}(\vec{q}, \omega)$  and  $\hat{S}_{\mathcal{X}\mathcal{X}}(\vec{q}, \omega)$  at various temperature for wave vectors  $\vec{q} = 0$  and  $\vec{q} = (\pi/10a, 0, 0)$ . HD denotes the central peak due to heat diffusion, and C the central peak arising from the cluster dynamics. ss denotes the second-sound peak, and oss overdamped second sound.

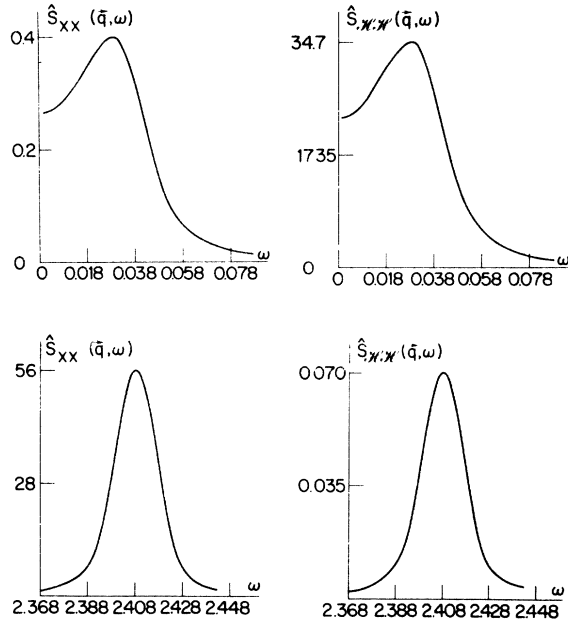


FIG. 5.  $\hat{S}_{xx}(\vec{q}, \omega)$  and  $\hat{S}_{xcxc}(\vec{q}, \omega)$  at  $k_B T = 0.5$  for  $\vec{q} = (\pi/10, 0, 0)$ .

hibits a CP peak with half-width  $\Delta\omega \sim q^2$ , due to heat diffusion. This phenomenon does not occur in  $\hat{S}_{xx}$ , as expected, because the displacement-energy coupling vanishes above  $T_c$ . Moreover, the broad phonon resonance shifts to lower frequencies with decreasing temperature. At  $k_B T = 8$ , which is close to  $k_B T_c \approx 7.1$ , new features appear: a CP at  $\vec{q} = (0, 0, 0)$  in  $\hat{S}_{xx}$  and the soft mode becomes overdamped. At  $\vec{q} = \vec{0}$ , heat diffusion does not exist. Consequently, the  $\vec{q} = \vec{0}$  CP must be attributed to the cluster dynamics. In  $\hat{S}_{xcxc}$ , it is superimposed by the Rayleigh peak.

Below  $T_c$ , the coupling between displacement and energy fluctuations is nonzero. The Rayleigh peak will appear, therefore, in both  $\hat{S}_{xx}$  and  $\hat{S}_{xcxc}$ . Accordingly, we have at  $k_B T = 6$  and  $\vec{q} = 0$ , the Rayleigh and cluster central peaks superimposed. The cluster CP also appears, as is seen from  $\vec{q} = \vec{0}$ . The soft mode is overdamped. At  $k_B T = 4$ , the soft mode becomes underdamped and the height of the cluster CP is reduced, as expected. In fact, for the formation of clusters, it is necessary that particles overcome the potential barrier. This process becomes less probable as the temperature is lowered. This fact is illustrated at  $k_B T = 2$ , where the cluster CP no longer appears ( $\vec{q} = \vec{0}$ ). At  $\vec{q} \neq \vec{0}$  there is a CP due to the energy fluctuations in both  $\hat{S}_{xx}$  and  $\hat{S}_{xcxc}$ , but it is weak in  $\hat{S}_{xx}$ . The  $\vec{q}$  dependence of the half-width reveals, however, that this CP cannot be explained in terms of heat diffusion. Since this peak splits at lower temperatures ( $k_B T$

$= 1$ ), it must be attributed to overdamped second sound. The phonon resonance is now defined, indicating that we enter the regime where anharmonic perturbation theory should work. At  $k_B T = 1$ , the phonon is very well defined. It dominates  $\hat{S}_{xx}$ , but at small  $\omega$  the weak second-sound resonance appears. This peak dominates  $\hat{S}_{xcxc}$ , where the phonon peak is very weak. At the lower temperature  $k_B T = 0.5$ , the features are similar to those at  $k_B T = 1$ . The only difference is a zero-frequency tail of the second-sound resonance in  $\hat{S}_{xcxc}$ . This tail must be attributed to two phonon processes, arising from the first term in Eq. (19). Finally, at  $T = 0$ , where the spectrum can be calculated exactly, only the phonon resonance survives [Eqs. (70) and (75)].

To substantiate and illustrate this overview, we next discuss the excitation spectrum in more detail. Figure 5 shows the  $\omega$  dependence of  $\hat{S}_{xx}(\vec{q}, \omega)$  and  $\hat{S}_{xcxc}(\vec{q}, \omega)$  for  $\vec{q} = (\pi/10a, 0, 0)$  at  $k_B T = 0.5$ . The phonon resonance at  $\omega = 2.42$  is very well defined and appears in both  $\hat{S}_{xx}$  and  $\hat{S}_{xcxc}$ , due to the coupling between order-parameter and energy fluctuations [cf. Eqs. (59) and (60)]. The coupling term is  $a_{34}$  given by Eq. (38). In agreement with Green's function approach, the phonon resonance is weak in  $\hat{S}_{xcxc}$  and strong in  $\hat{S}_{xx}$ . At low frequency, there is an additional well-defined peak which might be second sound. In Sec. IIC, where the occurrence of this collective excitation was assumed, certain of

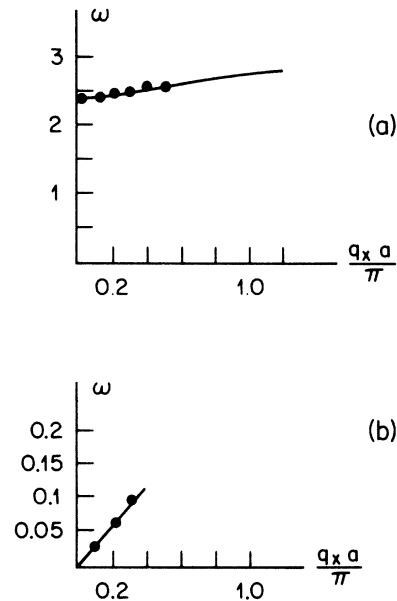


FIG. 6. Calculated dispersion law at  $k_B T = 0.5$ . (a) phonon branch [the full line represents the high-frequency approximation result (52) with  $\langle X_i^2 \rangle$  taken from Table I]; (b) second-sound branch.

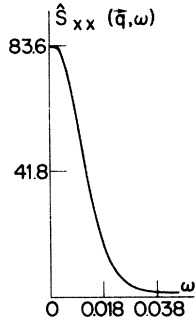


FIG. 7.  $\hat{S}_{xx}(\vec{q}, \omega)$  at  $k_B T = 6$  for  $\vec{q} = \vec{0}$ .

its properties were estimated. According to Eqs. (59) and (60), it should occur as a weak resonance in  $\hat{S}_{xx}$  and as a strong peak in  $\hat{S}_{\mathcal{J}\mathcal{C}\mathcal{J}\mathcal{C}}$ , in accordance with Fig. 5. A further prediction relates to the second-sound velocity  $C_{ss}$ , given by Eq. (67). Setting  $\omega_A = 2.42$ , we obtain the estimate

$$C_{ss} \frac{\pi}{a} = 0.31, \tag{129}$$

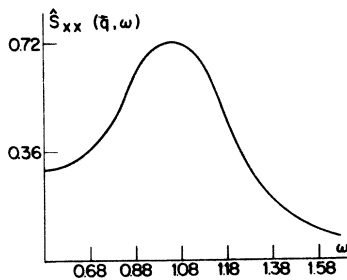
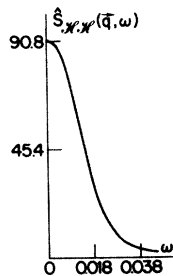
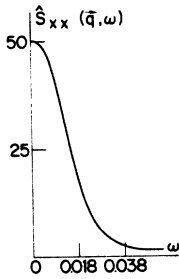
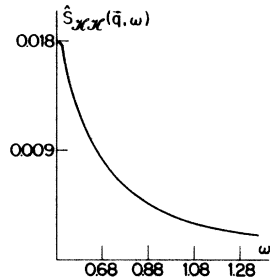


FIG. 8.  $\hat{S}_{xx}(\vec{q}, \omega)$  and  $\hat{S}_{\mathcal{J}\mathcal{C}\mathcal{J}\mathcal{C}}(\vec{q}, \omega)$  at  $k_B T = 6$  for  $\vec{q} = (\pi/10a, 0, 0)$ .

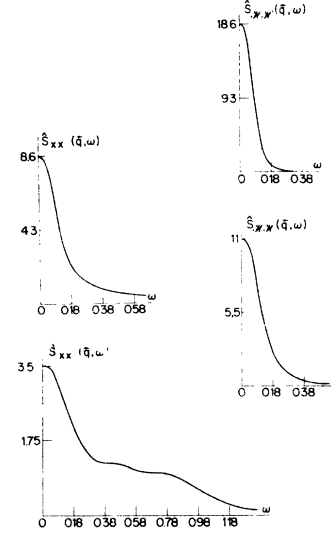


FIG. 9.  $\hat{S}_{xx}(\vec{q}, \omega)$  and  $\hat{S}_{\mathcal{J}\mathcal{C}\mathcal{J}\mathcal{C}}(\vec{q}, \omega)$  at  $k_B T = 8$  for  $\vec{q} = (\pi/10a, 0, 0)$ .

leading to the frequency

$$\omega = 0.1 \cdot C_{ss} \pi / a = 0.031, \tag{130}$$

at  $q_{\text{reduced}} = q\pi/a = 0.1$ . This estimate is in very good agreement with the peak at  $\omega = 0.028$ . We conclude, therefore, that the low-frequency peak is due to second sound.

Figure 6 shows the dispersion relation derived from the peak maxima in  $\hat{S}_{xx}$  and  $\hat{S}_{\mathcal{J}\mathcal{C}\mathcal{J}\mathcal{C}}$ . The phonon frequencies agree very well with the high-frequency estimates based on Eq. (52) (full line) which have been included for comparison. The straight line in Fig. 6(b) represents the estimated second-sound velocity Eq. (129); evidently it fits the numerical data very well. The second peak is found to decrease in intensity and its half-width to increase with increasing wave vector.

As discussed in the overview and sketched in Fig. 4, second sound becomes overdamped around  $k_B T = 2$ . This is illustrated in Fig. 7, showing the  $\omega$  dependence of  $\hat{S}_{xx}(\vec{q}, \omega)$  and  $\hat{S}_{\mathcal{J}\mathcal{C}\mathcal{J}\mathcal{C}}(\vec{q}, \omega)$  at  $k_B T = 2$  for  $\vec{q} = (\pi/10a, 0, 0)$ . Consequently, well-defined second sound occurs only in the temperature window below  $T_c$ .

Around  $k_B T = 4$ , a new feature sets in, namely, a CP at  $\vec{q} = \vec{0}$ . This is illustrated in Fig. 7, for  $k_B T = 6$ . Since the half-width of the CP, due to heat diffusion, is proportional to  $q^2$ , the  $\vec{q} = \vec{0}$  peak must be attributed to the cluster dynamics. At finite  $\vec{q}$ , the cluster CP is superimposed on the heat-diffusion peak. This situation is illustrated in Fig. 8. Obviously, the superimposed central peaks are the dominating feature in both  $\hat{S}_{xx}$  and  $\hat{S}_{\mathcal{J}\mathcal{C}\mathcal{J}\mathcal{C}}$ . The strength of the additional peak around  $\omega = 1.08$  in

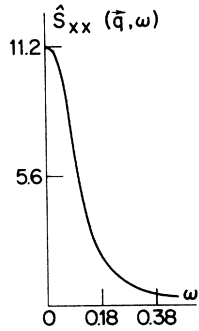


FIG. 10.  $\hat{S}_{xx}(\vec{0}, \omega)$  at  $k_B T = 8$ .

$\hat{S}_{xx}(\vec{q}, \omega)$  is very small, so that the phonon is essentially overdamped. The small intensity of the phonon contribution indicates that on approaching  $T_c$  and for small wave vectors, the phonon branch disappears from the scene. For larger wave vectors it gradually appears and becomes well defined near the zone boundary.

Above  $T_c$ , energy and displacement fluctuations are no longer coupled. As a consequence, heat diffusion will no longer give rise to a CP in  $\hat{S}_{xx}$ . Figure 9 shows the  $\omega$  dependence of  $\hat{S}_{xx}$  and  $\hat{S}_{xxc}$  at  $k_B T = 8$  for  $\vec{q} = (\pi/10a, 0, 0)$ . Due to the reasons mentioned above, the CP in  $\hat{S}_{xx}$  is only a result of the cluster dynamics. Its counterpart in  $\hat{S}_{xxc}$ , however, is still a superposition of heat diffusion and cluster peaks. The cluster contribution is il-

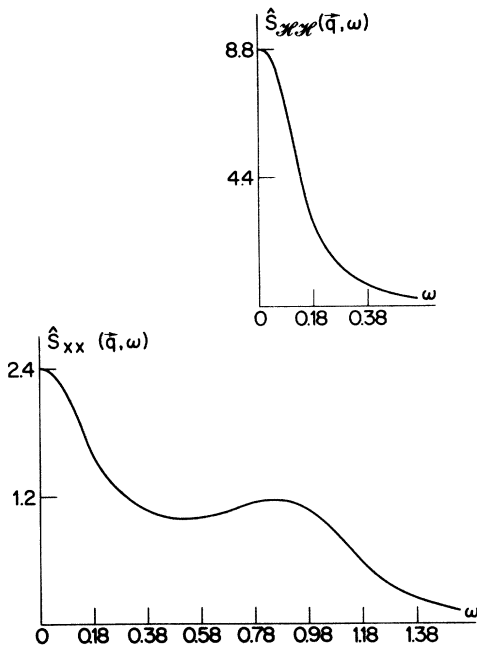


FIG. 11.  $\hat{S}_{xx}(\vec{q}, \omega)$  and  $\hat{S}_{xxc}(\vec{q}, \omega)$  at  $k_B T = 8$  and  $\vec{q} = (2\pi/5a, 0, 0)$ .

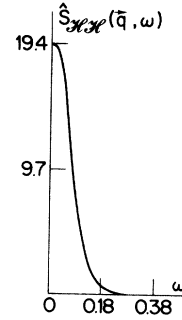


FIG. 12.  $\hat{S}_{xx}(\vec{q}, \omega)$  and  $\hat{S}_{xxc}(\vec{q}, \omega)$  at  $k_B T = 15$  and  $\vec{q} = (\pi/10a, 0, 0)$ .

lustrated in Fig. 10, showing  $\hat{S}_{xx}(\vec{0}, \omega)$ . Figure 9 also reveals that on approaching  $T_c$  from above, the phonon becomes overdamped for small wave vectors. It becomes better defined for larger wave vectors, as is seen in Fig. 11. Finally, we consider  $k_B T = 15$ . Here, we no longer observe a central peak in  $\hat{S}_{xx}(\vec{0}, \omega)$  because at high temperatures the jump frequency over the potential barrier becomes quite large. Consequently, the CP in  $\hat{S}_{xxc}$  for  $\vec{q} \neq \vec{0}$ , as shown in Fig. 12, is only due to heat diffusion.  $\hat{S}_{xx}$  no longer exhibits a CP but a broad "phonon" peak.

Finally, we turn to the critical slowing down. According to the universality hypothesis for dynamic critical phenomena,<sup>4</sup> one expects that our system should become equivalent to a purely relaxational time-dependent Ginzburg-Landau model with conserved energy. Accordingly, the characteristic time of the order-parameter fluctuations is expected to diverge as<sup>4</sup>

$$\begin{aligned} \tau_{xx} &= \int_0^\infty \langle X(-\vec{q}, t)X(-\vec{q}, 0) \rangle dt / \langle X(-\vec{q}, 0)X(-\vec{q}, 0) \rangle \\ &= B^2 |\epsilon|^{-\Delta}, \end{aligned} \quad (131)$$

where

$$\epsilon = (T - T_c)/T_c, \quad (132)$$

TABLE II. Numerical estimates of the characteristic time Eq. (131) and of the amplitudes  $B^-(T < T_c \approx 7.1)$  and  $B^+(T > T_c)$ .

$T$	$ \epsilon $	$\tau_{xx}$	$B^\pm = \tau_{xx} \epsilon ^{1.4}$
4	0.44	15	4.8
5	0.30	35	6.5
6	0.15	84	5.9
8	0.13	17	0.98
8.5	0.20	12	1.26
9	0.27	9	1.44

$$\Delta = \nu(2 + \alpha/\nu) . \quad (133)$$

$\nu$  is the critical exponent of the correlation length and  $\alpha$  of the specific heat. According to the universality hypothesis for static properties, which we discussed in Sec. IIIA,  $\nu$  and  $\alpha$  should be identical to the corresponding exponents of the three-dimensional Ising model, namely,<sup>24</sup>

$$\nu \approx 0.638, \quad \alpha \approx \frac{1}{8} , \quad (134)$$

yielding

$$\Delta \approx 1.4 . \quad (135)$$

Our results are summarized in Table II. Since the limited data do not allow an estimate of  $\Delta$ , we have taken the above value and calculated the amplitudes  $B^+$  and  $B^-$ , yielding

$$B^+/B^- \approx 4.7 . \quad (136)$$

The reasonable agreement between the values for  $B^+$  and  $B^-$ , respectively, suggest that the critical dynamics is indeed equivalent to that of the TDGL model with conserved energy.

### C. Nonlinear heat-pulse propagation

To study the propagation of heat pulses in the second-sound regime, we adopted the following procedure. The system, subjected to periodic boundary conditions, was brought into thermal equilibrium with temperature  $T$ . The particles in the first layer of two opposite planes of the cube were then brought into contact with a gas of particles having temperature  $T_p$  and mass  $M$ . After switching off this contact, we followed the propagation of the resulting temperature pulse, characterized by the distribution of the kinetic energy of the particles. The heat source was simulated by assuming collisions between the gas and layer particles occurring at random time intervals  $t_i$ , distributed according to  $(1/\tau) \exp(-t_i/\tau)$ ,  $0 < t_i < \infty$ ,  $\tau$  being the mean time between two collisions. The resulting new momentum  $MX_i(t_i)$  of the  $i$ th layer particle was then chosen according to a Gaussian-distributed random number with variance  $Mk_B T_p$ .

This procedure was applied to any particle in the first layers of the two opposite planes of the unit cube. We chose  $\tau = \frac{1}{3}$  time units and the "heat source" was switched on over five time units. Consequently, there were 15 collisions per layer atom, on the average. The remaining part of the system was assumed to evolve according to the Langevin equations (108). As a consequence, this part of the system was in contact with a heat bath, and its temperature fixed correspondingly.

Figure 13 shows the propagation of the temperature pulse of initial height  $k_B T_p = 0.6$  with the aid of a hypsometric plot. The intensity of the blackening measures temperature and is discretized into four levels. The ambient temperature is  $k_B T = 0.125$ , lying within the second-sound regime. According to Eq. (103), the profile is represented by the kinetic energy in the  $l$ th plane, perpendicular to [100] in the cube. The profile is seen to propagate with velocity  $u$ , according to  $T = T(t - X/u)$ . It then collides with a pulse coming from the opposite side. The collision has some features reminiscent of solitons, i.e., the pulses penetrate one another without considerable change of shape or velocity but with a small phase shift, defined by

$$T(X, t) = T(t - X/u + \delta) .$$

An important difference with respect to the collision of solitons is the appearance of a localized pulse ( $u \approx 0$ ) after the collision. It should be borne in mind, however, that the system is a three-dimensional discrete lattice model, where infinitely long-lived solitons are unlikely.

To substantiate the solitonlike properties, we also estimated the relation between height and half-width of the profile before the collision occurred. The results are shown in Fig. 14. For small pulse heights, the prediction  $\Delta \sim H^{-1/6}$  [Eq. (107)] fits remarkably well. For higher pulses, however, systematic deviations occur. This indicates that the low-order expansion, outlined in Sec. IID, is reasonable for small amplitudes only. Nevertheless.

TABLE III. Profile velocities for various initial pulse heights  $k_B T_p$  at ambient temperature  $k_B T = 0.125$ . These values should be compared with the second-sound velocity  $C_{ss} \pi/a \approx 0.28$ .

$k_B T_p$	$u \pi/a$
0.2	0.30
0.4	0.31
0.6	0.32
0.8	0.33
1	0.33
1.2	0.33
1.4	0.35

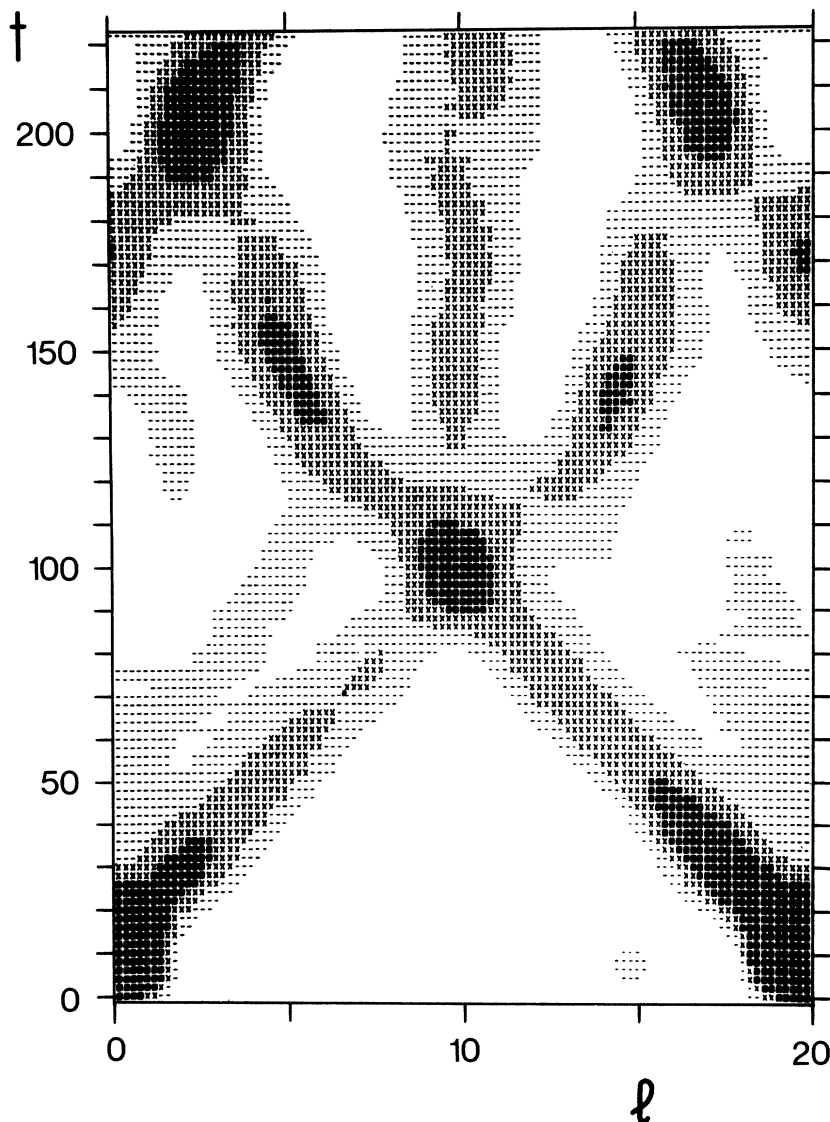


FIG. 13. Hypsometric plot of the temporal evolution of the temperature profile with initial height  $k_B T = 0.6$  at ambient temperature  $k_B T = 0.125$ . The intensity of the blackening measures temperature and is discretized into four levels. Temperature is measured in terms of the kinetic energy in the  $l$ th plane perpendicular to  $[100]$ .

for small amplitudes, the pulses propagate like the envelope solitons derived from the continuum version of the equation of motion [Eq. (103)].

From Table III, it is seen that the profile velocity  $u$ , evaluated before the collision, approaches the second-sound velocity if the initial pulse height  $T_p$  approaches the ambient temperature  $k_B T = 0.125$ .

At the upper limit of the temperature window, where second sound becomes overdamped, inherent nonlinearity becomes crucial because the formation of clusters sets in. Here the basic assumption underlying the derivation of envelope solitons breaks down. It is the assumption that the solution of the deterministic equation of motion is relevant in the statistical description of the sys-

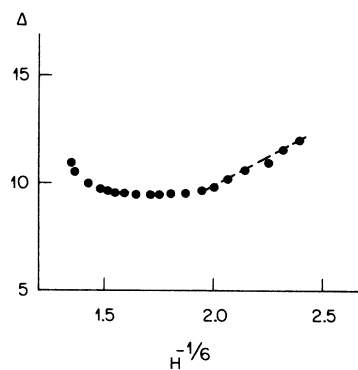


FIG. 14. Profile half-width  $\Delta$  vs height  $H$  to the power  $-\frac{1}{6}$  for  $k_B T = 0.125$ .

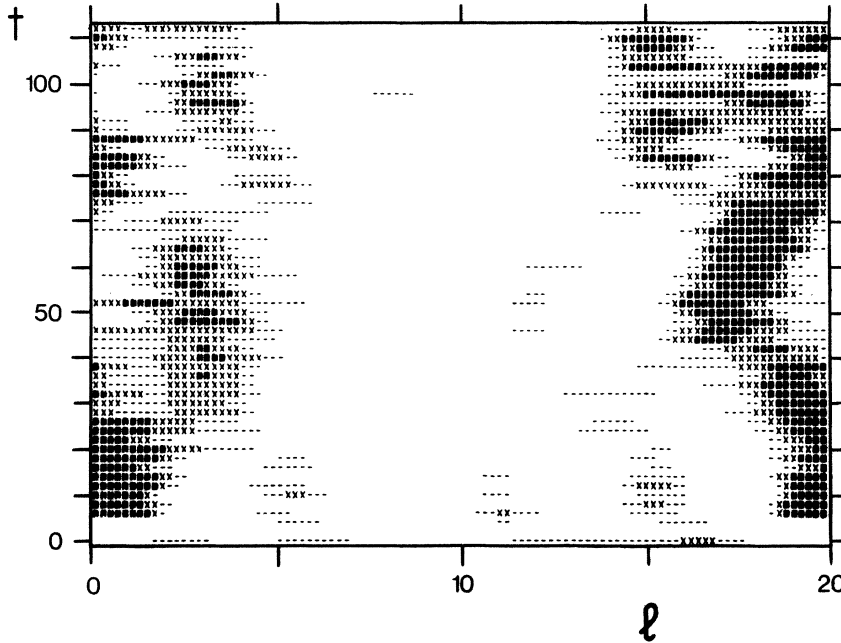


FIG. 15. Hypsometric plot of the temporal evolution of the temperature profile with initial height  $k_B T_p = 3$  at ambient temperature  $k_B T = 2$ .

tem. From the spectral densities, we know, however, that the local temperature fluctuations become purely relaxational above the upper window. Here, the local temperature fluctuations should be well described by the conventional heat-conduction equation

$$\frac{\partial T}{\partial t} = D \nabla^2 T. \quad (137)$$

This is illustrated in Fig. 15, showing the propagation of a temperature pulse with initial height  $k_B T_p = 3$  and ambient temperature  $k_B T = 2$ , where second sound is overdamped. There is no longer a solitonlike propagation. The pattern is in qualitative agreement, however, with the relevant solution of Eq. (137), namely,

$$T(x, t) = T_p (4D\pi t)^{-1/2} \exp(-X^2/4Dt) + T. \quad (138)$$

## V. SUMMARY AND CONCLUSIONS

The present study has revealed that nonlinearity and dispersion lead to a very rich excitation spectrum. Moreover, we have found that energy conservation and the nonvanishing coupling between order-parameter and energy fluctuations below  $T_c$  plays a crucial role.

At low temperature, anharmonic-perturbation theory applies. A well-defined optical mode exists and second sound occurs in a temperature window in both the energy and displacement spectral densities, due to the nonvanishing coupling between order-parameter and energy fluctuations. At the upper limit of the window, large-amplitude oscil-

lations set in, leading to the formation of clusters. Second sound becomes overdamped and changes over to heat diffusion, giving rise to the Rayleigh central peak. On approaching  $T_c$ , this CP is superimposed on a CP arising from the relaxational cluster dynamics, which also occurs at zero wave vector. The optical mode becomes overdamped and its weight in the spectral densities decreases as one approaches  $T_c$ . Above  $T_c$  heat diffusion occurs in the energy spectral density only, because energy and displacement fluctuations are no longer coupled. The CP in the displacement spectral density can be unambiguously traced back here to the cluster dynamics.

The critical slowing-down data are consistent with the universality hypothesis for dynamic phenomena, according to which the critical dynamics should be equivalent to that of the time-dependent Ginzburg-Landau model with conserved energy.

At very high temperatures, the system behaves like independent quartic anharmonic oscillations. Another interesting discovery was the envelope solitonlike propagation of heat pulses. This result and the demonstration of the cluster formation and cluster dynamics revealed that solitary wave and solitonlike behavior play an important role even in three-dimensional discrete lattices, where, however, they certainly have a finite lifetime only.

Finally, it might be appropriate to discuss the connection between the model which we have studied and real systems. There is considerable evidence that the static properties of distortive phase transitions are well described by anisotropic  $n$ -

component versions of the present model.<sup>1</sup> It then appears that even the one-component model considered in this work embodies some of the essential features of real systems. Nevertheless, one should bear in mind that these models are incompressible, due to the rigid reference lattice. Consequently, acoustical modes and their interaction with the order-parameter fluctuations are either lacking or taken into account in terms of an adiabatic approximation. In any case, they would also affect the static properties.

The fact that our model is that of a pure system appears to be more crucial. As the history of the experimental work on second sound reveals,<sup>9</sup> to produce equivalent real systems may be a lengthy procedure.

#### ACKNOWLEDGMENTS

The authors are indebted to A. D. Bruce and H. Thomas for valuable suggestions on this work. Furthermore we thank R. H. Morf for implementing the random number generator.

#### APPENDIX: INTEGRATION OF THE LANGEVIN EQUATIONS

The integration technique of the Langevin equation

$$m_i \ddot{\vec{X}}_i = -\nabla_i V(\vec{X}_1, \dots, \vec{X}_N, t) - \Gamma M \dot{\vec{X}}_i + \vec{\eta}_i(t) \quad (\text{A1})$$

will be subdivided into the following parts: (A) integration of the deterministic equation; (B) modifications due to the presence of damping; and (C) introduction of the random-noise source.

##### A. Integration of the deterministic equations

We write our system of coupled differential equations in the following form:

$$m_i \ddot{\vec{X}}_i = -\nabla_i V(\vec{X}_1, \vec{X}_2, \dots, \vec{X}_N, t), \quad (\text{A2})$$

where the subscript  $i$  refers to particle  $i$  with mass  $m_i$ . Including the presence of external forces, the potential  $V$  may be explicitly time dependent. In this section, however, we confine ourselves to conservative forces. Thus,  $V$  is taken to be independent of the particle velocities  $\dot{\vec{X}}_i$ . This suggests the use of a numerical scheme which does not require the knowledge of first derivatives.

A simple formula<sup>25</sup> can be derived from a Taylor expansion of  $\vec{X}_i(t \pm \Delta)$  up to third derivatives

$$\begin{aligned} \vec{X}_i(t + \Delta) &= \vec{X}_i(t) + \Delta \dot{\vec{X}}_i(t) + \frac{1}{2} \Delta^2 \ddot{\vec{X}}_i(t) \\ &\quad + \frac{1}{6} \Delta^3 \dddot{\vec{X}}_i(t) + O(\Delta^4) \end{aligned} \quad (\text{A3})$$

and

$$\begin{aligned} \vec{X}_i(t - \Delta) &= \vec{X}_i(t) - \Delta \dot{\vec{X}}_i(t) + \frac{1}{2} \Delta^2 \ddot{\vec{X}}_i(t) \\ &\quad - \frac{1}{6} \Delta^3 \dddot{\vec{X}}_i(t) + O(\Delta^4). \end{aligned} \quad (\text{A4})$$

Adding these two quantities we get, as in Ref. 26,

$$\vec{X}_i(t + \Delta) + \vec{X}_i(t - \Delta) = 2\vec{X}_i(t) + \Delta^2 \ddot{\vec{X}}_i(t) + O(\Delta^4). \quad (\text{A5})$$

Let us investigate its stability properties for the harmonic oscillator problem

$$V(\vec{X}_i) = \frac{1}{2} m \omega_0^2 \vec{X}_i^2. \quad (\text{A6})$$

Using the ansatz

$$\vec{X}_i(t) = e^{i\alpha t + \beta t} \vec{e}, \quad (\text{A7})$$

where  $\alpha$  and  $\beta$  are real constants and  $\vec{e}$  is a unit vector, we obtain together with the equation of motion (A5),

$$e^{i\alpha\Delta + \beta\Delta} = -e^{-i\alpha\Delta - \beta\Delta} + 2 - \Delta^2 \omega_0^2 \quad (\text{A8})$$

or

$$\cos \alpha \Delta \cosh \beta \Delta = 1 - \frac{1}{2} \Delta^2 \omega_0^2 \quad (\text{A9})$$

and

$$\sin \alpha \Delta \sinh \beta \Delta = 0. \quad (\text{A10})$$

To discuss the solutions to these equations, we have to consider three different cases:

$$(i) \quad \Delta \alpha \neq n\pi, \quad n = 0, \pm 1, \pm 2, \dots$$

In this case,  $\beta$  has to be zero and the solution is thus stable. Thus, the approximation only leads to phase errors which result in a frequency shift. The frequency  $\alpha$  is found to be

$$\alpha = (1/\Delta) \arccos(1 - \frac{1}{2} \Delta^2 \omega_0^2), \quad (\text{A11})$$

and for small  $\Delta \omega_0$ ,

$$\alpha \approx \omega_0 (1 + \frac{1}{24} \Delta^2 \omega_0^2); \quad (\text{A12})$$

$$(ii) \quad \Delta \alpha = 2n\pi, \quad n = 0, \pm 1, \dots$$

Equation (A9) in this case becomes

$$\cosh \beta \Delta = 1 - \frac{1}{2} \Delta^2 \omega_0^2 \quad (\text{A13})$$

which for nonzero  $\omega_0$  has no real solution for  $\beta$ .

For  $\omega_0 = 0$  we get the correct result  $\beta = 0$ .

$$(iii) \quad \Delta \alpha = (2n+1)\pi, \quad n = 0, \pm 1, \pm 2, \dots$$

In this case, Eq. (A9) is

$$\cosh \beta \Delta = \frac{1}{2} (\Delta \omega_0)^2 - 1, \quad (\text{A14})$$

which has no real solution as long as  $\Delta \omega_0 < 2$ . For  $\Delta \omega_0 > 2$  we find unstable solutions with  $\beta > 0$ .

Thus, the stability limit is given by

$$\Delta \omega_0 = 2. \quad (\text{A15})$$

The finite difference approximation is thus stable as long as

$$\Delta < T/\pi, \quad (\text{A16})$$

where  $T$  is the period of oscillation.

The numerical procedure defined by Eq. (A5) is not self-starting because it requires the knowledge of both  $\vec{X}(-\Delta)$  and  $\vec{X}(0)$ . In initial-value problems, where  $\vec{X}(0)$  and its derivative are defined,  $\vec{X}(-\Delta)$  must be calculated using Eqs. (A2) and (A4).

The dynamical initial conditions, i.e.,  $\dot{\vec{X}}_i(t=0)$ ,  $\ddot{\vec{X}}_i(t=0)$  are not generally known. Instead we have prescribed values of thermodynamic quantities, e.g., temperature, density, number of particles, etc. In order to generate corresponding initial states,  $\Gamma$  must not be chosen too small in order to reach equilibrium in a reasonable time interval. To avoid artifacts owing to a particular choice of  $\Gamma$  and of the random force, equilibrium is best reached by stepwise decreasing values of  $\Gamma$ .

#### B. Equations of motion with damping

In contrast to the situation considered above, here the equations of motion explicitly depend on the velocities  $\dot{\vec{X}}_i$ ,

$$m_i \ddot{\vec{X}}_i = -\nabla_i V(\vec{X}_1, \dots, \vec{X}_N, t) - \Gamma m_i \dot{\vec{X}}_i. \quad (\text{A17})$$

The velocities  $\dot{\vec{X}}_i$  are eliminated from Eq. (A17) by introducing new variables

$$\vec{y}_i = e^{\Gamma t/2} \dot{\vec{X}}_i. \quad (\text{A18})$$

Then Eq. (A17) becomes

$$\ddot{\vec{y}}_i = \frac{1}{4} \Gamma \dot{\vec{y}}_i - e^{\Gamma t/2} (1/m_i) \nabla_i V(\vec{X}_1, \vec{X}_2, \dots, \vec{X}_N, t). \quad (\text{A19})$$

This equation can now be integrated by means of Eq. (A5),

$$\vec{y}_i(t+\Delta) = 2\vec{y}_i(t) - \vec{y}_i(t-\Delta) + \Delta^2 \ddot{\vec{y}}_i(t) + O(\Delta^4), \quad (\text{A20})$$

or inserting the definition of  $\vec{y}_i$ ,

$$\begin{aligned} \vec{X}_i(t+\Delta) &= 2\vec{X}_i(t) e^{-\Gamma\Delta/2} - e^{-\Delta\Gamma} \vec{X}_i(t-\Delta) + \Delta^2 e^{-\Gamma\Delta/2} \\ &\times \left[ \frac{1}{4} \Gamma^2 \vec{X}_i(t) - (1/m_i) \nabla_i V(\vec{X}_1, \dots, \vec{X}_N, t) \right] \\ &+ O(\Delta^4). \end{aligned} \quad (\text{A21})$$

This equation, although of order  $\Delta^4$  like Eq. (A5), has a serious deficiency; it is not translationally invariant. However, this can be corrected by re-writing Eq. (A21) as

$$\begin{aligned} \vec{X}_i(t+\Delta) &= \vec{X}_i(t) + [\vec{X}_i(t) - \vec{X}_i(t-\Delta)] e^{-\Gamma\Delta} \\ &- \Delta^2 e^{-\Gamma\Delta/2} (1/m_i) \nabla_i V(\vec{X}_1, \dots, \vec{X}_N, t) \\ &+ O(\Delta^4). \end{aligned} \quad (\text{A22})$$

This equation is identical to Eq. (A21) up to third order in  $\Delta$ . Furthermore, it displays translational invariance.

#### C. Introduction of the random-noise source

The stochastic force  $\vec{\eta}_i(t)$  in Eq. (11) is a Gaussian-distributed random vector. Its  $\alpha$  component has the following property:

$$\langle \eta_i^\alpha(t) \eta_k^\alpha(t+\tau) \rangle = 2m_i k_B T \Gamma \delta_{ik} \delta(\tau). \quad (\text{A23})$$

Here,  $k_B$  denotes the Boltzmann constant, and  $T$  stands for the temperature of the heat bath on which our system is coupled by  $\Gamma$ . In a Gauss-Markov process, the times  $t_i$  between two random-noise pulses are distributed as

$$p(t_i) = (1/\tau) \exp(-t_i/\tau), \quad (\text{A24})$$

where  $\tau$  is the mean time between two pulses. In a system with a discrete time-interval grid of time steps  $\Delta$ , the probability  $p$  that after  $\Delta$  one random pulse acts, is given by

$$p = \int_0^\Delta p_i(t) dt = 1 - \exp\left(-\frac{\Delta}{\tau}\right) \approx \frac{\Delta}{\tau}. \quad (\text{A25})$$

An ansatz that satisfies Eqs. (A23) and (A25) is

$$\eta_i^\alpha(t) = A \sum_j \delta(t-t_j) \gamma_i^\alpha(t_j) \Theta(p - a_{0ij}^\alpha). \quad (\text{A26})$$

$j$  labels the time steps,  $\gamma_i^\alpha(t_j)$  is a Gaussian-distributed random number, and  $a_{0ij}^\alpha$  is a random number equally distributed between 0 and 1. Introducing Eq. (A26) in (A23) and averaging over a long time period  $T$ , we get

$$\begin{aligned} \langle \eta_i^\alpha(t) \eta_k^\beta(t+\tau) \rangle_T &= \lim_{T \rightarrow \infty} \frac{1}{T} \int_0^T dt A^2 \sum_{j,j'} \delta(t-t_j) \delta(t-t_{j'}+\tau) \\ &\times \langle \gamma_i^\alpha(t_j) \gamma_k^\beta(t_{j'}) \Theta(p - a_{0ij}^\alpha) \Theta(p - a_{0kj'}^\beta) \rangle. \end{aligned} \quad (\text{A27})$$

The properties of the Gaussian random numbers  $\gamma_i^\alpha(t_j)$  lead to the relation

$$\begin{aligned} \langle \gamma_i^\alpha(t_j) \gamma_k^\beta(t_{j'}) \Theta(p - a_{0ij}^\alpha) \Theta(p - a_{0kj'}^\beta) \rangle \\ = p \delta_{\alpha\beta} \delta_{ik} \delta_{jj'}. \end{aligned} \quad (\text{A28})$$

Therefore, Eq. (A27) can be written

$$\begin{aligned} \langle \eta_i^\alpha(t) \eta_k^\beta(t+\tau) \rangle &= \lim_{T \rightarrow \infty} \frac{A^2}{T} \int_0^T dt \sum_j \delta(t-t_j) \\ &\times \delta(t-t_j+\tau) p \delta_{\alpha\beta} \delta_{ik} \\ &= \lim_{N \rightarrow \infty} \frac{A^2}{N\Delta} p N \delta_{ik} \delta_{\alpha\beta} \delta(\tau), \end{aligned} \quad (\text{A29})$$

where  $T = N\Delta$ .

Comparing Eqs. (A29) and (A23), we get for  $A$ ,

$$A = [2m_i k_B T \Gamma \Delta / p]^{1/2}, \quad (\text{A30})$$

and introducing this value in Eq. (A26) leads to

$$\eta_i^\alpha(t) = [2m_i k_B T \Gamma \Delta / p]^{1/2} \times \sum_j \delta(t-t_j) \gamma_i^\alpha(t_j) \Theta(p - a_{0ij}^\alpha). \quad (\text{A31})$$

The properties of the  $\delta$  function can now be used to integrate Eq. (A1) over a time interval  $t_j - \epsilon$  to  $t_j + \epsilon$  and  $\epsilon \rightarrow 0$ ,

$$\int_{t_j - \epsilon}^{t_j + \epsilon} \dot{\bar{X}}_i dt' = \int_{t_j - \epsilon}^{t_j + \epsilon} \bar{\eta}_i(t') \frac{dt'}{m_i} + O(\epsilon). \quad (\text{A32})$$

The left parts read  $\dot{\bar{X}}_i(t+0^*) - \dot{\bar{X}}_i(t-0^*)$ . So we find for the velocities

$$\begin{aligned} \dot{X}_i^\alpha(t_j+0^*) &= \dot{X}_i^\alpha(t_j-0^*) + [k_B T \Gamma \Delta / p m_i]^{1/2} \\ &\quad \times \gamma_i^\alpha(t_j) \Theta(p - a_{0ij}^\alpha) \\ &= \dot{X}_i^\alpha(t_j-0^*) + \delta \dot{X}_i^\alpha. \end{aligned} \quad (\text{A33})$$

The second term depends on  $\Gamma$  where, according to Eq. (A1),

$$\delta \dot{X}_i^\alpha(t) = \delta \dot{X}_i^\alpha(0) e^{-\Gamma t}, \quad (\text{A34})$$

so that

$$\begin{aligned} \delta X_i^\alpha(t + \Delta) &= \delta \dot{X}_i^\alpha(0) \int_0^\Delta e^{-\Gamma t} dt = \delta \dot{X}_i^\alpha(0) \frac{1 - e^{-\Gamma \Delta}}{\Gamma} \\ &\approx \delta \dot{X}_i^\alpha(0) \Delta e^{-\Gamma \Delta / 2}. \end{aligned} \quad (\text{A35})$$

Using  $\delta X_i^\alpha(t + \Delta)$  introduced in Eqs. (A22) and (A33), we find

$$\begin{aligned} \bar{X}_i(t + \Delta) &= \bar{X}_i(t) + [\bar{X}_i(t) - \bar{X}_i(t - \Delta)] e^{-\Gamma \Delta} - \Delta^2 e^{-\Gamma \Delta / 2} \\ &\quad \times (1/m_i) [\nabla_i V(\bar{X}_1, \dots, \bar{X}_N, t) \\ &\quad + (m_i k_B T \Gamma / \Delta p)^{1/2} \\ &\quad \times \bar{\gamma}_i(t) \Theta(p - \bar{a}_{0i})], \end{aligned} \quad (\text{A36})$$

where the  $\alpha$  components of  $\gamma^\alpha$  and  $a_{0i}^\alpha$  are collected as vectors.

The random part in Eq. (A36) now acts as a rectangular function in the acceleration with height  $(m_i k_B T \Gamma / \Delta p)^{1/2}$ , over the interval between  $-\frac{1}{2}\Delta$  and  $+\frac{1}{2}\Delta$ . These folding properties show that a Gauss-Markov process is simulated only if  $2\pi/\Delta$  is much larger than the frequencies for which the spectral densities are different from zero.

The Gaussian-distributed random numbers can be combined from a set of 12 random numbers equally distributed between zero and one (Ref. 27),

$$\gamma = \sum_{k=1}^{12} a_{0k} - 6.0. \quad (\text{A37})$$

To create the random numbers  $a_{0k}$  we used the

power residue method (Ref. 28)

$$u_i = Xu_{i-1} \pmod{2^b}; \quad (\text{A38})$$

$u_0$  and  $X$  must be odd numbers,

$$a_{0i} = u_i / 2^b. \quad (\text{A39})$$

These pseudorandom numbers have good random properties in the left-hand-side figures. The right-hand-side figures are correlated. To obtain reasonable randomness with only marginal repeating parts, we have chosen  $b = 64$ ,  $X = 2^{32} + 3$  belonging to the odd-number subclass  $8t + 3$ , and for  $u_0$  an odd number corresponding to the time and date to start with uncorrelated noise initials.

In equilibrium systems, the mean-square velocity of one component corresponds to temperature. For calculations of  $\bar{X}_i$  and its mean square, we approximate the tangent at  $t$  by a secant through the points  $t - \Delta$  and  $t + \Delta$ ; these approximations lead to second-order correction terms of  $\Delta$  in  $\langle \dot{X}_i^2 \rangle$ . The random noise on the other hand, involves first-order corrections which may be taken into account,

$$\dot{\bar{X}}_{i \text{ calc}}(t) = [\bar{X}_i(t + \Delta) - \bar{X}_i(t - \Delta)] / 2\Delta t. \quad (\text{A40})$$

Using Eq. (A33), we observe that the mean square at  $t$  has two parts,

$$\langle [\bar{X}_i(t)]^2 \rangle = \frac{1}{2} \langle [\bar{X}_i(t - 0^*)]^2 \rangle + \frac{1}{2} \langle [\bar{X}_i(t + 0^*)]^2 \rangle. \quad (\text{A41})$$

Combining Eqs. (A41), (A33), and (A28), we obtain

$$\langle [\dot{X}_i^\alpha(t)]^2 \rangle = \langle [\dot{X}_i^\alpha(t - 0^*)]^2 \rangle + (1/m_i) k_B T \Gamma \Delta, \quad (\text{A42})$$

and, together with Eq. (A40),

$$\langle [\dot{\bar{X}}_i^\alpha(t)]^2 \rangle = \langle [\dot{\bar{X}}_{i \text{ calc}}^\alpha]^2 \rangle + (1/2m_i) k_B T \Gamma \Delta. \quad (\text{A43})$$

In equilibrium, when we can assume that

$$\langle [X_i^\alpha(t)]^2 \rangle = k_B T, \quad (\text{A44})$$

we then get

$$\langle [\dot{\bar{X}}_i^\alpha(t)]^2 \rangle = \frac{\langle [\dot{\bar{X}}_{i \text{ calc}}^\alpha]^2 \rangle}{1 - \frac{1}{2}\Gamma \Delta}. \quad (\text{A45})$$

A further condition is that the distribution of  $\delta \dot{X}_i^\alpha$  is much smaller than the Boltzmann distribution of the particles, and using Eqs. (A44) and (A31) we obtain

$$k_B T \Gamma (\Delta / p m_i) \ll k_B T / m_i \quad (\text{A46})$$

and

$$\Gamma \Delta \ll \frac{1}{2} p. \quad (\text{A47})$$

<sup>1</sup>A. D. Bruce, *Ferroelectrics* **12**, 21 (1976).

<sup>2</sup>M. E. Fisher, *Rev. Mod. Phys.* **46**, 597 (1974).

<sup>3</sup>S. Sarbach, T. Schneider, and E. Stoll, *Phys. Rev. B* **10**, 2004 (1974).

<sup>4</sup>B. I. Halperin, in *Proceedings of the International Conference on Statistical Physics, Budapest, 1975*, edited by L. Pál and P. Szépfalusy (North-Holland, Amsterdam, 1976).

- <sup>5</sup>T. Schneider and E. Stoll, Phys. Rev. Lett. 31, 1254 (1973).
- <sup>6</sup>T. Schneider and E. Stoll, Phys. Rev. B 13, 1216 (1976).
- <sup>7</sup>H. Mori, Prog. Theor. Phys. 33, 423 (1965); 34, 399 (1965).
- <sup>8</sup>P. F. Meier, Phys. Kondens. Mater. 17, 17 (1973).
- <sup>9</sup>V. Narayanamurti and C. M. Varma, Phys. Rev. Lett. 25, 1105 (1970).
- <sup>10</sup>F. D. Tappert and C. M. Varma, Phys. Rev. Lett. 25, 1108 (1970).
- <sup>11</sup>H. Beck, in *Dynamical Properties of Solids*, edited by G. K. Horton and A. A. Maradudin (North-Holland, Amsterdam, 1974), Vol. II, p. 205.
- <sup>12</sup>C. P. Enz, Rev. Mod. Phys. 46, 705 (1974).
- <sup>13</sup>St. Sarbach, Phys. Rev. B 15, 2694 (1977).
- <sup>14</sup>T. Schneider, H. Beck, and E. Stoll, Phys. Rev. B 13, 1123 (1976).
- <sup>15</sup>J. A. Krumhansl and J. R. Schrieffer, Phys. Rev. B 11, 3535 (1975).
- <sup>16</sup>C. M. Varma, Phys. Rev. B 14, 244 (1976).
- <sup>17</sup>V. Narayanamurti, R. C. Dynes, and K. Andres, Phys. Rev. 11, 2500 (1975).
- <sup>18</sup>R. K. Bullough, in *Interaction of Radiation with Condensed Matter* (IAEA, Vienna, 1977), p. 381.
- <sup>19</sup>A. C. Scott, F. Y. F. Chu, and D. W. McLaughlin, Proc. IEEE 61, 1443 (1973).
- <sup>20</sup>T. Taniuti and N. Yajima, J. Math. Phys. 10, 1369 (1969).
- <sup>21</sup>F. P. Tappert and R. H. Hardin, SIAM Rev. 13, 283 (1971).
- <sup>22</sup>R. Morf and E. Stoll, in *Numerical Analysis*, edited by J. Descloux and J. Marti (Birkhäuser, Basel, 1977), ISNM Vol. 37, p. 139.
- <sup>23</sup>A. Aharony and P. C. Hohenberg, Phys. Rev. B 13, 3081 (1976).
- <sup>24</sup>D. S. Gaunt and C. Domb, J. Phys. C 3, 1442 (1970).
- <sup>25</sup>S. K. Godunov and V. S. Ryabenki, *Theory of Difference Schemes (An Introduction)* (North-Holland, Amsterdam, 1964), p. 47.
- <sup>26</sup>C. Verlet, Phys. Rev. 159, 98 (1967).
- <sup>27</sup>R. W. Hamming, in *Numerical Methods for Scientists and Engineers* (McGraw-Hill, New York, 1962), pp. 34 and 384.
- <sup>28</sup>IBM Manual, C20-8011, *Random Number Generation and Testing* (IBM, White Plains, N. Y., 1959).